ILMATIETEEN LAITOS
METEOROLOGISKA INSTITUTET
FINNISH METEOROLOGICAL INSTITUTE

FINNISH METEOROLOGICAL INSTITUTE

77

CONTRIBUTIONS

REMOTE SENSING OF SNOW-COVER FOR THE BOREAL FOREST ZONE USING MICROWAVE RADAR

KARI LUOJUS

FINNISH METEOROLOGICAL INSTITUTE
CONTRIBUTIONS
No. 77

Remote Sensing of Snow-Cover for the Boreal Forest Zone Using Microwave Radar

Dissertation for the degree of Doctor of Science in Technology

Kari Luojus

Dissertation for the degree of Doctor of Science in Technology to be presented with due permission of the Faculty of Electronics, Communications and Automation, for public examination and debate in Auditorium S4 at Helsinki University of Technology (Espoo, Finland) on the 15th of May, 2009, at 12 noon.

Finnish Meteorological Institute
Helsinki, 2009

Distribution:
Finnish Meteorological Institute
P.O.Box 503
FIN-00101 Helsinki
Finland

Tel. +358 9 1929 4683
Fax +358 9 1929 4603

Email: kari.luojus@fmi.fi

ISBN 978-951-697-689-4 (paperback)
ISBN 978-951-697-690-0 (pdf)
ISSN 0782-6117
http://lib.tkk.fi/Diss/2009/isbn9789516976900/

Yliopistopaino
Helsinki 2009

FINNISH METEOROLOGICAL INSTITUTE

Published by Finnish Meteorological Institute
(Erik Palménin aukio 1) , P.O. Box 503
FIN-00101 Helsinki, Finland

Series title, number and report code of publication
Finnish Meteorological Institute Contributions 77
FMI-CONT-77

Date April 2009

Author

Kari Luojus

Title

Remote Sensing of Snow-Cover for the Boreal Forest Zone Using Microwave Radar

Abstract

This doctoral dissertation describes the development of an operationally feasible snow monitoring methodology utilizing spaceborne synthetic aperture radar (SAR) imagery, intended for hydrological applications on the boreal forest zone. The snow-covered area (SCA) estimation methodology developed is characterized using extensive satellite-based datasets, including SAR-based estimation and optical reference data gathered during the snow-melt seasons of 1997-1998, 2000-2002 and 2004-2006 from northern Finland. The methodology applies satellite-based C-band SAR data for snow monitoring during the spring snow-melt season. The SCA information can be utilized for river discharge forecasting and flood predictions and for the optimization of hydropower production.

The development efforts included 1) demonstration of a forest compensation algorithm, 2) establishing the use of wide-swath SAR data 3) development of a weather station assimilation procedure and 4) creation of an enhanced reference image selection algorithm for the SCA estimation methodology.

The feasibility of a proposed, non-boreal forest specific, SAR-based SCA estimation method was evaluated for the boreal forest zone. The acquired results were compared with the characteristics determined for the boreal-forest specific methodology developed within this dissertation. These results can be used when selecting appropriate SCA estimation approaches for future snow monitoring systems whether conducted in different regions or intended for larger i.e. continental or global scale purposes.

An automatic processing system for SCA estimation was developed and demonstrated as part of this work; the system has been delivered to the Finnish Environment Institute for operational use.

Publishing unit
Arctic research

Classification (UDK)
551.501.86 551.578.46 551.579.2

Keywords
remote sensing, snow monitoring
snow-covered area, synthetic aperture radar

ISSN and series title
0782-6117 Finnish Meteorological Institute Contributions

ISBN
978-951-697-689-4 (paperback), 978-951-697-690-0 (pdf)

Language
English

Sold by
Finnish Meteorological Institute / Library
P.O.Box 503, FIN-00101 Helsinki
Finland

Pages
178

ILMATIETEEN LAITOS

Julkaisija Ilmatieteen laitos, (Erik Palménin aukio 1)
PL 503, 00101 Helsinki

Julkaisun sarja, numero ja raporttikoodi
Finnish Meteorological Institute Contributions 77
FMI-CONT-77

Julkaisuaika Huhtikuu 2009

Tekijä

Kari Luojus

Nimeke

Lumipeitteen kaukokartoitus havumetsävyöhykkeellä mikroaaltotutkan avulla

Tiivistelmä

Väitöskirjatyössä kehitetään synteettisen apertuurin tutkan (SAR) satelliittikuviin perustuvaa lumenseurantamenetelmää, joka soveltuu operatiiviseen hydrologiseen käyttöön havumetsä-vyöhykkeellä. Kehitetty lumenpeittoalan (SCA) estimointimenetelmä karakterisoitiin käyttäen laajoja satelliittikuva aineistoja: SAR-tutka- ja optisia satelliittikuvatulkintoja lumen sulamiskausilta 1997-1998, 2000-2002 ja 2004-2006 Pohjois-Suomesta. Menetelmä hyödyntää C-taajuuskaistan satelliitti SAR-tutkakuvia lumen sulamisen seurantaan kevätsulantakaudella. Lumen sulantatietoa voidaan hyödyntää jokien virtaamaennusteiden ja tulvaennusteiden laadintaan sekä vesivoimatuotannon optimointiin.

Kehitystyö on sisältänyt 1) metsäkompensointialgoritmin demonstroinnin 2) laajan peittoalan SAR-tiedon hyödyntämismenetelmien kehityksen 3) sääasemaassimilaatio-menetelmän kehittämisen 4) parannetun referenssikuva valinta-algoritmin kehittämisen, lumenpeittoalan estimointimenetelmään.

Lisäksi vuoristoalueille kehitetyn lumenpeittoalan estimointimenetelmän käyttökelpoisuutta tutkittiin havumetsäalueella; saatuja tuloksia verrattiin väitöskirjatyössä kehitetyn havumetsä alueille soveltuvan menetelmän tuloksiin. Menetelmien vertailutuloksia voidaan hyödyntää lumenpeittoala menetelmien valinnassa liittyen eri alueille tai erilaisissa mittakaavoissa toteutettaviin järjestelmiin.

Osana väitöskirjatyötä kehitettiin ja demonstroitiin automaattinen prosessointijärjestelmä lumenpeitto-alan estimointiin; järjestelmä on otettu operatiiviseen käyttöön Suomen ympäristökeskuksessa.

Julkaisijayksikkö
Arktinen tutkimus

Luokitus (UDK)
551.501.86 551.578.46 551.579.2

Asiasanat
kaukokartoitus, lumen monitorointi
lumenpeittoala, synteettisen apertuurin tutka

ISSN ja avainnimike
0782-6117 Finnish Meteorological Institute Contributions

ISBN
978-951-697-689-4 (nidottu), 978-951-697-690-0 (pdf)

Kieli
Englanti

Myynti
Ilmatieteen laitos / Kirjasto
PL 503, 00101 Helsinki

Sivumäärä
178

PREFACE

The research presented in this dissertation was carried out in the legendary, (nowadays the former), Laboratory of Space Technology at the Helsinki University of Technology, during 2004-2008. The endeavor was multifaceted with its evident ups and downs as expected for the sort of journeys that last for several years. Although the work comes to a certain conclusion with the printing of this dissertation, I've always said that it is not concluded by any means; this simply marks an intermediate stepping stone for a journey that has just gotten a relatively nice start.

Although the dissertation was written by me and carries my name, it is only a part of a bigger picture. The work presented here would never have happened without the support and help from a large number of people, both at the laboratory and at home.

On the academic side, my foremost appreciation goes to my mentor, Prof Jouni Pulliainen, who guided and helped me through this journey. The work conducted for this dissertation carries as much a telltale signature from Jouni as from the first author. My other great instructor, Prof Martti Hallikainen, is also gratefully acknowledged for providing support and guidance in the field of remote sensing. And for the AVA-family (a great bunch of talented, diverse and, dare I say, "crazy" people) we had at the legendary Laboratory of Space Technology, thank you for making every day at the "AVA-labra" a reason to be grateful. We sure had our fair share of immemorial parties as well. I am also grateful to Sari Metsämäki and Saku Anttila of the Finnish Environment Institute for the fruitful collaboration in our various snow research projects.

For financial support I would like to thank the Tekniikan Edistämissäätiö, the Jenny and Antti Wihuri Foundation, the Walter Ahlström Foundation and the Graduate School of Electrical and Communications Engineering of TKK.

Probably the most important factor in my success has been my family at home. My words cannot express my gratitude for my mother Eeva-Liisa, my brother Timo and my father Tapani; you have made me what I am, and given me the opportunity and support to chase my dreams in life.

Finally, I want to thank my wife Mirja for making it possible for me to pursue my academic dreams; this accomplishment is yours as much as mine; although we both know that this one is rather insignificant when compared to Neea, Samu and Arttu.

For me the conclusion of a great project has always meant a start of a new one, sometimes an even greater one; and the future, I predict, will certainly not pale in comparison with the past.

Vantaa, April 2009

Kari Luojus

TABLE OF CONTENTS

LIST OF ACRONYMS AND SYMBOLS

Acronyms

AIEM	Advanced Integral Equation Model
ASAR	Advanced Synthetic Aperture Radar (instrument on board Envisat)
AVHRR	Advanced Very High Resolution Radiometer
CEOS	Committee on Earth Observation Satellites
DEM	Digital Elevation Model
DMRT	Dense Medium Radiative Transfer
Envisat	ESA operated satellite, launched in 2002
EO	Earth Observation
ESA	European Space Agency
ERS-1	European Remote-Sensing Satellite 1, launched in 1991
ERS-2	European Remote-Sensing Satellite 2, launched in 1995
FMI	Finnish Meteorological Institute
FSC	Fractional Snow-Covered Area
HH	Horizontal-Horizontal (H-transmitting and H-receiving polarizations)
HUTSCAT	Helsinki University of Technology Scatterometer
HV	Horizontal-Vertical (H-transmitting and V-receiving polarizations)
IEM	Integral Equation Model
MAE	Mean Absolute Error
MODIS	Moderate Resolution Optical Imaging Spectroradiometer
NASA	National Aeronautics and Space Administration (USA)
NOAA	National Oceanic and Atmospheric Administration (USA)
Radarsat-1	Canadian, SAR-equipped satellite, launched in 1995
Radarsat-2	Canadian, SAR-equipped satellite, launched in 2007
RMS	Root Mean Square
RMSE	Root Mean Square Error
SAR	Synthetic Aperture Radar
SCA	Snow-Covered Area (*standing for the fractional SCA*)
SCW	ScanSAR Wide (imaging mode of Radarsat-1 SAR)
SD	Snow Depth
SWE	Snow Water Equivalent
SYKE	Finnish Environment Institute
TKK	Helsinki University of Technology, Finland
TM	Thematic Mapper (instrument on board Landsat-satellite)
VH	Vertical-Horizontal (V-transmitting and H-receiving polarizations)
VV	Vertical-Vertical (V-transmitting and V-receiving polarizations)
WSFS	Watershed Simulation and Forecasting System
WSM	Wide-Swath Medium resolution (imaging mode of Envisat ASAR)

Symbols

ε_g	soil dielectric constant
θ	incidence angle
θ_t	transmission angle
θ_s	reflection angle
λ	wavelength
μ_s	cos of the scattering angle
ϕ_s	azimuth angle
ρ	snow density
ω	snow volume scattering albedo
τ	optical depth
σ	radar cross section
σ°	differential backscattering coefficient, backscattering coefficient
σ^o_{can}	forest canopy backscattering contribution
σ^o_{ground}	backscattering coefficient from the snow-free ground
σ^o_{obs}	the observed backscattering coefficient
σ^o_{ref}	the reference backscattering coefficient
σ^o_{snow}	backscattering coefficient from the snow-covered ground
$\sigma^o_{snow\text{-}air}$	backscattering contribution from the snow-air interface
$\sigma^o_{snow\text{-}ground}$	backscattering contribution from the snow-ground interface
$\sigma^o_{snow\text{-}vol}$	volume scattering contribution from the snow pack
σ^o_{surf}	backscattering coefficient of the ground or snow layer
A_{ill}	radar illuminated area
d_0	effective snow grain size
G	antenna gain
h	snowpack thickness
I_p	incident or scattered power intensity
I_{pp}	scattering intensity term
k	wave number
k_x	k cos θ
k_z	k sin θ
l	horizontal snow surface correlation length
$m_{v,snow}$	snow wetness
n	number of stem volume classes
p_1, p_2	polarization coefficients

P_{pp}	phase function of volume scattering
P_t	transmitted power
P_t	received power
R	distance between the antenna and the target
t^2	two-way transmissivity through forest canopy
T_{lt}	Fresnel power transmission coefficient
TR	threshold
s_s	snow surface RMS-height
s_g	ground surface RMS-height
S^2_{SCA}	variance of the SCA estimate
$S^2_{\sigma^\circ surf}$	variance of the observed surface backscattering coefficient
$S^2_{\sigma^\circ ground,ref}$	variance of the snow free ground backscattering coefficient
$S^2_{\sigma^\circ snow,ref}$	variance of the snow-covered ground backscattering coefficient
V	forest stem volume
w_i	weighing factor for a stem volume class
W	surface correlation function

LIST OF APPENDED PAPERS

This dissertation is based on the work contained in the following publications, hereafter referred to as publications [P1] to [P6]:

[P1] **K. Luojus**, J. Pulliainen, S. Metsämäki and M. Hallikainen, "Accuracy Assessment of SAR Data-Based Snow-Covered Area Estimation Method", IEEE Transactions on Geoscience and Remote Sensing, vol. 44, no. 2, pp. 277-287, February 2006.

[P2] **K. Luojus**, J. Pulliainen, S. Metsämäki and M. Hallikainen, "Snow-Covered Area Estimation Using Satellite Radar Wide-Swath Images", IEEE Transactions on Geoscience and Remote Sensing, vol. 45, no. 4, pp. 978-989, April 2007.

[P3] **K. Luojus**, J. Pulliainen, S. Metsämäki and M. Hallikainen, "Enhanced SAR-Based Snow-Covered Area Estimation Method for Boreal Forest Zone", IEEE Transactions on Geoscience and Remote Sensing, vol. 47, no. 3, pp. 922-935, March 2009.

[P4] **K. Luojus**, J. Pulliainen, A. Blasco Cutrona, S. Metsämäki and M. Hallikainen, "Comparison of SAR-based Snow-Covered Area Estimation Methods for the Boreal Forest Zone", IEEE Geoscience and Remote Sensing Letters, vol. 6, no. 3, pp. 403-407, July 2009.

[P5] J. Koskinen, J. Pulliainen, **K. Luojus** and M. Takala, "Monitoring of Snow Cover Properties During the Spring Melting Period in Forested Areas", IEEE Transactions on Geoscience and Remote Sensing, (accepted for publication).

[P6] **K. Luojus** and J. Pulliainen, "Automatic Processing Chain for SAR Data-Based Snow-Covered Area Estimation Method", Helsinki University of Technology, Laboratory of Space Technology, Report No. 65, Espoo, Finland, November 2006, 33 pages. Editor: M. Hallikainen (TKK).

In [P1]-[P4] and [P6] the first author was responsible for carrying out the research presented. The other authors acted as scientific advisors, gave ideas and processed or produced data. In [P5] the research was performed in collaboration by J. Koskinen, J. Pulliainen and K. Luojus, the SAR data used were processed by K. Luojus.

1 INTRODUCTION

Seasonal snow cover is one of the most important elements of both the climate and hydrological system in the Northern Hemisphere. The extent of snow cover has been confirmed to be a sensitive climate change indicator; it influences the air temperature through positive albedo feedback and by insulation of soil from the atmosphere. Snow cover is also the main contributor to freshwater run-off in northern Hemisphere. The only feasible method for monitoring the snow cover on global scale is by utilizing satellite-based Earth observation (EO) information. Knowledge of the extent of snow cover can be utilized for various climatic, environmental, meteorological and hydrological applications, including such operative end use tasks as flood prevention and optimization of hydropower production, and the use of observational snow-cover information as validation input for climate models.

An essential variable for different end-use applications is the fraction of snow-covered area (SCA[1]) during the spring snow-melt season. Fractional SCA is being determined using various approaches on different regions of Northern Hemisphere. The traditional approach has been to interpolate temporally and spatially sparse observations from weather stations and snow courses. The conventional approach is inadequate in both temporal and spatial senses for most applications. Utilizing satellite-based earth-observation (EO) imagery large areas can be monitored on a daily- to weekly basis. Coverage can be extended to a global scale, or a selected region can be monitored with greater spatial resolution. Utilization of optical and microwave-based sensors will become even more important in the future as operational ground-based snow monitoring activities are being reduced in several countries.

EO-imagery can be acquired from different sensors. For snow monitoring applications, the available instruments utilize either the optical or microwave band of the electromagnetic spectrum. The optical band is divided into the visible band (wavelengths roughly 400nm to 700nm) and the infrared band (wavelengths roughly 700nm to 15 μm). The microwave band (wavelengths roughly 30 cm to 3 mm, translating to frequencies from 1 GHz to 100 GHz, respectively). The optical instruments utilized in nearly all cases use passive methods. The microwave instruments apply both active and passive methods for data acquisition. The passive microwave instruments are referred to as radiometers and the active sensors are called radars. There are several types of radars: those utilized from spaceborne platforms are either Synthetic Aperture Radars (SAR) or scatterometers. Scatterometers and radiometers can typically cover significantly larger areas, but with a coarser resolution than SAR instruments. For global and continental scale Earth observation, the utilization of scatterometers or radiometers is feasible and widely practiced. For regional applications, the high spatial resolution achieved by SAR from spaceborne platforms makes them the optimal solution for snow-melt monitoring, along with optical sensors. The largest difference between optical and SAR instruments is the requirement for cloud-free conditions and the need for solar illumination for optical

[1] The acronym SCA used throughout this dissertation, refers to a fractional snow-covered area value, not a binary value (snow vs. no snow), as used by some investigators. The acronym (FSC) utilized by some colleagues is equivalent to the acronym SCA, that is used within this dissertation.

measurements. For operational use, optical data are therefore severely limited, as there can be significant periods of time during the snow-melt season, with no data from a monitored target area. SAR is an active instrument and utilizes the microwave band of the electromagnetic spectrum. Electromagnetic radiation at microwave frequencies is very little affected by the atmosphere and can be operated in practically all-weather conditions and during day and night. Operational end-users utilizing snow information for hydrological or weather forecasting purposes desire access to high resolution, accurate and operationally available data. Optical data can be acquired when weather conditions permit. Scatterometer and radiometer data are too coarse for typical hydrological applications.

To fulfill the requirements of operational end-users, spaceborne SAR data are perhaps the best candidate for snow monitoring applications. Modern-day operational snow monitoring systems often utilize both optical and SAR data, as the high cost and somewhat limited availability of SAR imagery (the availability issue was more highlighted in the past) can be easily complemented using optical data.

Table 1-1. A list of current and past non-military spaceborne SAR instruments. (The temporary Shuttle based SIR-A, SIR-B, SIR-C, SRTM are not included as they were only operated for the duration of the STS missions.)

Satellite (launch year)	Currently operational (Apr. 2009)	Center frequency (band)	Polarizations	Incidence angle (degrees from vertical)
Seasat (1978)	No	1.275 GHz (L-band)	HH	23
Almaz-1 (1991)	No	3.125 GHz (S-band)	HH	30 – 60
ERS-1 (1991)	No	5.3 GHz (C-band)	VV	23
JERS-1 (1992)	No	1.275 GHz (L-band)	HH	38
ERS-2 (1995)	Yes	5.3 GHz (C-band)	VV	23
Radarsat-1 (1995)	Yes	5.3 GHz (C-band)	HH	20 - 49
Envisat (2002)	Yes	5.3 GHz (C-band)	HH, VV, HV, VH (Dual polarization)	15 – 45
ALOS (2006)	Yes	1.27 GHz (L-band)	HH, VV, HV, VH (Fully polarimetric)	8 – 60
TerraSAR-X (2007)	Yes	9,65GHz (X-band)	HH, VV, HV, VH (Dual polarization)	15 – 60
COSMO-Skymed (2007)	Yes	9,65GHz (X-band)	HH, VV, HV, VH (Dual polarization)	20 – 60
Radarsat-2 (2007)	Yes	5.3 GHz (C-band)	HH, VV, HV, VH (Fully polarimetric)	20 – 49

Additionally, optical data are in many cases available free of charge; for example data from many National Aeronautics and Space Administration (NASA) and National Oceanic and Atmospheric Administration (NOAA) sensors, such as the Advanced Very High Resolution Radiometer (AVHRR) or the Moderate Resolution Optical Imaging Spectroradiometer (MODIS) are distributed free of charge for end-users.

A list of current and past spaceborne SAR instruments is shown in Table 1.1. The current and past spaceborne SAR instruments have operated between L- and X-bands (frequencies between 1.27 GHz to 9.65 GHz). The C-band SAR data have been most widely available (ERS-1 and -2, Radarsat-1 and -2 and Envisat) and therefore the largest body of snow investigations from spaceborne instruments and the developed operational SAR-based snow monitoring system are based on C-band data. The launches of TerraSAR-X and Cosmo-Skymed (which will eventually be a constellation of 4 satellites) have improved the availability of X-band data, but they are not yet as easily and widely available as the C-band imagery. Partly due to these aspects (data availability) partly the excellent feasibility of C-band SAR for snow monitoring applications, the investigations within this dissertation are focused on the C-band SAR. The spaceborne scatterometer data have also been available from Ku-band (frequencies between 12 GHz and 18 GHz) and these data have been investigated for coarse resolution snow monitoring. The typically low spatial resolution (tens of kilometers) achieved from scatterometers does, however, not provide a basis for accurate regional applications.

1.1 Operational snow monitoring using Earth observation data

The satellite-based snow monitoring systems implemented for operational use are predominantly based on optical sensors (*Hall et al. 1995, 1998, Vikhamar and Solberg 2003, Salomonson and Appel 2004, Metsämäki et al. 2002, 2005*). Although viable in many ways, the optical methods do have some severe drawbacks. The most significant limitation of optical remote sensing is the need for solar illumination and cloud-free conditions, which are further magnified at high latitudes. Since the temporal resolution achieved is partly dependent on weather conditions, it is possible that there are long periods without valid data during the often rapidly progressing snow-melt season. These difficulties can be overcome by radar remote sensing means, which are not limited by weather or solar illumination.

The feasibility of synthetic aperture radar (SAR) for snow monitoring during the spring snow-melt season has been widely investigated. There are several factors that make SARs advantageous in remote sensing of snow. The main benefits are the high spatial resolution (from 5 to 100 meters on C-band, depending on instrument and imaging mode and up to 1 meter in X-band), weather independence and the temporal and spatial coverage achieved. The spatial coverage is dependent on the imaging mode, with up to 500 km x 500 km image size on current spaceborne SAR instruments. Temporal resolution depends on the latitude, imaging mode and instrument; it typically ranges from one day to one week.

Several methods for SCA estimation have been established using spatially limited SAR imagery for various regions (*Rott 1984, Rott and Nagler 1993, Koskinen et al. 1994, Piesbergen et al. 1995, Guneriussen et al. 1996, Shi and Dozier 1997, Koskinen et al. 1997, Nagler and Rott 2000*). The basic research for SCA estimation on boreal forest regions has been carried out at TKK and it is presented in (*Koskinen et al.*

1997) and (*Pulliainen et al. 2001*). The further development of the TKK method is a key topic of this dissertation.

One of the key requirements for an operational EO-system in addition to the achieved temporal coverage and accuracy is the spatial coverage. Most SAR-based snow-covered area monitoring systems have originally been developed using spatially limited data, typically covering areas smaller than 100 km x 100 km. For global use and for many regional applications this is inadequate. Using wide-swath SAR instruments, such as Radarsat-1 or Envisat ASAR, it is possible to attain significantly wider coverage. The Radarsat-1 ScanSAR Wide A (SCW) imaging mode produces SAR images with 500 km x 500 km spatial coverage. For example, a single image covers northern Finland completely. However, the application for large areas using wide-swath SAR imagery introduces a challenge. The detected radar backscattering signature is dependent on the incidence angle of the image element (*Ulaby et al. 1982, Baghdadi et al. 2000, Magagi and Bernier 2003*). In a SCW image the incidence angle varies between 20° and 49°. Since the estimation of SCA is dependent on the backscattering signature, it is essential to determine whether the estimation of SCA using images with largely varying incidence angle is feasible. The issue has been investigated for mountainous regions (*Storvold and Malnes 2004*). The validation of wide-swath SAR utilization for SCA estimation for the boreal forest zone is investigated and presented within this dissertation.

Optimal results for operational snow monitoring applications can be achieved by combining the EO imagery from both optical and SAR instruments. There are several possible ways to combine the data from different sensors. The methodology for assimilating different EO-based data sources are beyond the scope of this dissertation and only considered here for a few example cases. Demonstration of snow cover retrieval from multi-parameter airborne SAR and SPOT HRV was presented in (*Raggam et. al 1994*). Time-series analysis using NOAA AVHRR and ERS-2 SAR images was presented in (*Koskinen et al. 1999*). However, in these cases there was no actual combination of the two data other than studying how the snow-cover progress could be monitored by the two sensors. A successful methodology for combining Envisat ASAR and Terra/MODIS data was demonstrated in (*Solberg et. al 2004*). The methodology was further refined and one of the modern state-of-the-art snow monitoring system, assimilating both optical and SAR-based data, is presented in (*Solberg et al. 2008*).

In addition to optical and SAR-based methods, global scale (low-resolution) snow monitoring (snow depth, snow water equivalent and extent of dry snow) can be carried out using passive microwave instruments, e.g. (*Chang et al. 1987, Hallikainen and Jolma 1992*) and lower resolution active instruments such as scatterometers, see, for example, (*Nghiem and Tsai 2001, Hallikainen et al. 2005, Tedesco and Miller 2007*). The utilization of these methods for snow-melt monitoring on regional scale is however not feasible due to their limited accuracy and coarse spatial resolution, and their limited applicability to monitoring of wet snow.

1.2 Contribution of this dissertation to SAR-based snow monitoring

Monitoring of snow cover parameters can be carried out using a wide range of instruments and methodologies. For this dissertation, the work is focused on C-band spaceborne SAR, which can provide reliable snow cover information for hydrological simulation and forecasting applications for operational use on a regional scale.

The main objectives of the work presented in this dissertation were:

(1) to develop an operationally feasible SAR-based SCA estimation methodology for boreal forest region [P1], [P2], [P3],

(2) to characterize the accuracy of SCA estimation for the boreal forest zone using the developed methodology [P1], [P2], [P3],

(3) to develop a feasible method for producing uncertainty information for the SCA estimates and to investigate the automation of the SCA estimation method, including the development of an demonstration system that can be utilized in operational hydrological monitoring [P2], [P6],

(4) to evaluate the feasibility of the existing SAR-based SCA estimation methods for the boreal forest zone [P4] and to improve the understanding of the behavior of snow backscattering signatures during the snow-melt season [P5].

The objectives 1)-3) are effectively targeted to produce a methodology for operational SCA estimation on boreal forest zone that can be employed in hydrological simulation and forecasting applications. The objective 4) is targeted to increase the basic knowledge on SAR-based snow remote sensing.

Chapter 2 introduces the theoretical background of radar remote sensing, explains the observed temporal variance of radar backscattering signature utilized on snow monitoring and presents the snow-covered area estimation methods that are based on temporal changes of the radar backscattering signature during the snow-melt season.

Chapter 3 describes the work carried out for the advancement of snow monitoring methodologies using spaceborne SARs. The work described within this chapter is published in [P1]-[P6].

Chapter 4 presents the conclusions from the dissertation.

Chapter 5 includes the summaries of the appended papers.

2 ESTIMATION OF THE FRACTION OF SNOW-COVERED AREA (SCA) FROM SPACEBORNE SAR DATA

This Chapter introduces the theoretical background of radar remote sensing, explains the observed temporal variance of radar backscattering signature utilized on snow monitoring and presents the snow-covered area estimation methods that are based on temporal changes of the radar backscattering signature during the snow-melt season.

2.1 Synthetic aperture radar

Synthetic aperture radar (SAR) is an active microwave instrument. It functions by transmitting electromagnetic waves and measuring the scattered electromagnetic signal from the target. The SAR is an instrument consisting of a transmitter, an antenna, a receiver and data handling equipment. Typical remote sensing radars function in the microwave region of the electromagnetic spectrum, which is divided into several different bands (*IEEE Std. 2002*):

- L-band (1 GHz – 2 GHz)
- S-band (2 GHz – 4 GHz)
- C-band (4 GHz – 8 GHz)
- X-band (8 GHz – 12 GHz)
- Ku-band (12 GHz – 18 GHz)
- K-band (18 GHz – 27 GHz)
- Ka-band (27 GHz – 40 GHz)

Spaceborne radars up to now have functioned in a frequency range of 1.2 GHz to 9.65 GHz (from L-band to X-band), see Table 1.1. The main benefit of microwave instruments functioning between L- and X-bands is the ability to obtain measurements regardless of clouds and solar illumination in almost all weather conditions. The higher the utilized frequency, the more weather phenomena affect the measurements. At X-band and lower frequencies, the effects of atmospheric weather phenomena and cloud cover can be neglected. The radar measurements are typically categorized by the frequency used, and the transmitted and received polarizations.

The polarization is determined by the alignment of the electric vector in the transmitted or received electromagnetic wave. Radars are typically designed to transmit either horizontally or vertically polarized radiation. Reception can also be performed in horizontal or vertical or both polarizations. The polarizations are referred as H for horizontal and V for vertical. Radar that transmits and receives using the same polarization is known as co-polarization radar with a polarization of either HH as horizontal transmit and horizontal receive or VV as vertical transmit and vertical receive. Radar using cross-polarization transmits and receives in different polarizations, either VH or HV. Radar transmitting one polarization and measuring both polarizations are called dual-polarization radars. Polarimetric radar is able to transmit and receive on both vertical and horizontal polarizations (typically alternating between the two). The measurements include both the amplitude and phase information of the target, which are used to derive the polarimetric signature of the target (VV, HH, VH and HV polarizations and the phase differences for the co- and

cross-polarizations). The early spaceborne satellites measured only co-polarizations. Many of the current spaceborne radars are also capable of measuring dual-polarizations. The Radarsat-2 SAR, launched in 2007, is the only instrument capable of measuring full-polarization in the C-band. (See Table 1.1.) The spaceborne radars utilized in the snow-covered area estimation discussed within this dissertation function in co-polarization mode. The European Remote-Sensing Satellite 2 (ERS-2) SAR uses VV-polarization and the Radarsat-1 SAR uses HH-polarization. Both of them function in C-band at 5.3 GHz.

The SAR instrument transmits a signal and measures the signature scattered from the target. The actual variables that are measured are the intensity (power) and the phase of the backscattered signal. The phase can be used in interferometry applications, and the intensity information, which is more commonly used, expresses the magnitude of the backscattered signal. For spaceborne radars a monostatic setup is typically used, meaning that the transmitting and receiving antenna are the same. The equation for monostatic radar expressing the received power is written as (*Ulaby et al. 1982*)

$$P_r = \frac{P_t G^2 \lambda^2 \sigma}{(4\pi)^3 R^4} \tag{2-1}$$

where P_t is transmitted power, P_r is received power, G is antenna gain, λ is the wavelength and R is the distance between the antenna and the target. σ is the radar cross section. The intensity of backscattering is typically expressed as the average value the of backscattering cross section per unit area, which is referred to as *the differential backscattering coefficient* or the *backscattering coefficient*. The relation between the radar cross section and the *backscattering coefficient* is given by

$$\sigma^\circ = \left\langle \frac{\sigma}{A_{ill}} \right\rangle \tag{2-2}$$

where A_{ill} is the geometrical area of the illuminated target. The backscattering coefficient can be expressed using the radar equation (2.1) (*Ulaby et al. 1982*)

$$\sigma^\circ = \frac{P_r (4\pi)^3}{P_t \lambda^2} \cdot \frac{1}{\int_{Aill} \frac{G_n^2}{r^4}} \approx \frac{P_r (4\pi)^3}{P_t \lambda^2 G^2} \frac{r'^4}{A'_{ill}} \tag{2-3}$$

where G_n^2 is the antenna gain and A_{ill} is the radar-illuminated area. In the approximation r'^4 is the average distance from the illuminated area and A'_{ill} is the effective illuminated area. The approximation assumes that the distance from the target to the radar is constant within the illuminated area and that the antenna gain is constant within the beam width.

The radar measurements are usually expressed on a logarithmic scale. The logarithmic conversion is done by

$$\sigma^\circ_{dB} = 10 \log_{10} \sigma^\circ \tag{2-4}$$

Typical backscattering coefficients range between +5 dB (very bright) and – 30 dB (very dark). SAR data are typically illustrated using grayscale images where the different shades of grey are proportional to the intensity of the backscattering.

One of the key benefits of the SAR is the capability to achieve an excellent spatial resolution from a satellite platform. The spaceborne SAR instrument typically achieves a resolution of meters or tens of meters, depending on frequency and imaging mode. Radarsat-2, a modern day operational C-band SAR instrument, achieves a best resolution of 3 meters in both range and azimuth directions.

The range resolution is achieved using a pulse compression technique. A longer pulse with a frequency shift during the pulse is transmitted; when the backscattered pulse is analyzed it is passed through a delay line. The delay line delays the pulse according to its frequency. The frequency change of the pulse and the delay line are designed to compress the received pulse in time to allow for an enhanced range resolution.

The azimuth resolution emerges from the principles of synthetic aperture. The radar has a large beam width and observes a large area in the azimuth direction. Since the instrument moves relative to the ground, the backscattering signals received from targets with different azimuth distances have a relative Doppler shift with respect to each other. The instrument observes each target during the time it travels the distance of the beam width, and records all the backscattering information during this so-called synthetic aperture. The image processing system uses the recorded Doppler information to discriminate between different targets in the azimuth direction, thus the information for each image element is gathered throughout the synthetic aperture. The resulting azimuth resolution is equal to a real aperture instrument with the dimension of the synthetic aperture.

Modern spaceborne SAR instruments utilize different imaging modes. The spatial resolution achieved and the area covered by the image are dependent on the mode. The SAR instrument on Radarsat-1 can function in seven different imaging modes. The best spatial resolution of 9 x 9 meters is achieved using Fine Resolution mode; it produces images with a swath width of 50 km. The imaging mode optimal for operational snow monitoring is the ScanSAR mode. Using the ScanSAR Wide A (SCW) imaging mode the spatial resolution is 100 m in both range and azimuth directions and the swath width is 500 km. A typical SCW image has a size of 500 km x 500 km, which is very usable for monitoring of large areas (*RSI 2000*). The SAR instrument on ERS-2 satellite produces images with spatial resolution of 30 x 30 meters and an image size of 100 km x 100 km. Both instruments are very applicable for snow-covered area estimation, as shown in this dissertation.

2.2 Backscattering signatures of snow and ground

The backscattering coefficient measured by the radar is a sum of contributions from different scattering targets within the radar-illuminated area. Some backscattering signatures are born from interfaces where one medium changes into another (surface scattering); some are born from scatterers within a medium (volume scattering). In the case of snow remote sensing the main scattering contributions arise from the snow-air interface, volume scattering of snow and the snow-ground interface. The magnitudes of the different contributions are determined by snow properties, the polarization used, the frequency of the radar and the local incidence angle.

Remote sensing of snow on the boreal forest zone adds another ingredient to the equation: the forests. Backscattering contributions in addition to the ground-induced scattering are received from the crown layer, from tree trunks and from tree-ground

reflections. These are induced as surface scattering or volume scattering depending on the frequency of the radar.

The overall backscattering signature measured by the radar is a combination from multiple scattering sources and it is highly dependent on frequency, polarization and incidence angle. The backscattering perspective considered within this dissertation is regarded for C-band radar, approximately 5.3 GHz.

On C-band the backscattering of forest is significant and typically increases on forested areas with large stem volume content. The backscattering from snow is dependent on snow properties, the main factor being the amount and wetness of snow. Backscattering from ground layer is dependent on soil moisture and surface roughness. Remote sensing during the snow-melt season is based on the knowledge of the different backscattering signatures from snow and ground layers. The backscattering contribution of forests needs to be accounted for in the boreal forest zone, in order to acquire accurate information about the snow conditions.

2.2.1 Radar backscattering from snow

Snow is, in general, a mixture of ice crystals, liquid water and air. It is typically accumulated as a result of precipitation or wind deposition. The most basic parameters defining a snow layer are the density and the total thickness of the snow pack. Typically as the snow pack ages its density increases due to compaction by wind and gravity and through thermal metamorphism. The thickness of the snow layer and the snow density determine the snow water equivalent (SWE), which expresses the thickness of the water layer that would form if the snow pack were melted. The internal structure of snow pack is described by grain or crystal size. Grain size can be defined as the mean or equivalent radius of the ice crystals or the dominant size of the crystals. The following physical parameters affect the observed backscattering signature of a snow pack (*Hallikainen et al. 1986, Ulaby et al. 1986*):

- Liquid water content,
- Snow layer thickness,
- Snow layer density profile (the snow layer structure),
- Snow layer temperature profile,
- Surface roughness of the snow-air interface,
- Surface roughness of the snow-ground interface and
- Snow grain size (and shape).

Based on the quantity of liquid water in the mixture, snow is typically categorized into two types: (1) dry snow or (2) wet snow. Dry snow is a mixture of ice crystals and air, containing no liquid water. Wet snow is a mixture of dry snow and liquid water. The presence (or absence) of liquid water dominates the backscattering behavior of snow in the microwave region and also in the C-band (*Hallikainen et al. 1986, Ulaby et al. 1986*).

2.2.1.1 Dry snow

In the case of dry snow, the main contribution comes from the volume scattering from snow and the snow-ground interface. The C-band backscattering coefficient of dry

snow pack can increase, decrease or remain roughly constant as the snow water equivalent increases (*Ulaby et al. 1986, Strozzi et al. 1997, Shi and Dozier 2000*). The observed relation depends on particular snow and ground conditions.

The small difference between the dielectric constants of air and snow leads to a very small surface scattering component due to the small reflection and large power transmission coefficients. Therefore the surface roughness of dry snow makes almost no contribution to the overall backscattering (*Ulaby et al 1986*, *Shi and Dozier 2000*). The dielectric constant and surface scattering from dry snow increase as the snow density increases (*Hallikainen et al. 1986*). The backscattering coefficient decreases as the incidence angle increases (*Mätzler and Schanda 1984*), (*Ulaby et al 1986*). The snow-ground interface accounts for a significant amount of the backscattering signal from a dry snow pack (*Shi and Dozier 2000*).

2.2.1.2 Wet snow

As the snow wetness increases, the dielectric loss factor of snow increases (*Hallikainen et al. 1986*). This causes the absorption by the snow layer to increase and the backscattering contribution from the ground layer decreases. This results in a lower total backscattering coefficient from wet, snow-covered ground.

The backscattering of wet snow is highly dependent on the snow layer wetness and the surface roughness because of the major contribution from the snow-air interface. The backscattering coefficient typically decreases with increasing snow wetness (*Stiles and Ulaby 1980, Ulaby et al. 1986, Hallikainen et al. 1986, Fung 1994, Shi and Dozier 1995, Strozzi et al. 1997*).

The difference in backscattering between wet snow and dry snow increases with increasing incidence angle when the snow surface layer is smooth (*Ulaby et al. 1986, Guneriussen et al. 1996*). Typically the backscattering coefficient of wet snow increases with increasing frequency (*Arslan et al 2003*).

2.2.2 Radar backscattering from ground layer

Radar backscattering from a ground layer can be divided between the contributions from the soil layer and the vegetation (undergrowth).

The backscattering from a soil layer depends mainly on soil moisture, soil composition, soil temperature and surface geometry (surface roughness). In addition, the imaging parameters -incidence angle and polarization- have additional influence on the backscattering.

Considering only the effects of soil layer, the dominating factors are the soil moisture and surface roughness (*Ulaby et al. 1986, Hallikainen et al. 1985*). In C-band the radar backscattering increases as the volumetric soil moisture increases (*Hallikainen et al. 1985*). Additionally, the soil temperature determines the status of the moisture inclusions within the ground layer. Thawed soil can have a lower or a higher backscattering coefficient than frozen ground, depending on the soil type and its composition (*Hallikainen et al. 1985, Koskinen et al. 1997, Bernier et al. 1998*).

The effect of surface roughness depends on the incidence angle. At low incidence angles backscattering decreases as the surface roughness increases, whereas at high incidence angles the opposite is true: increasing surface roughness increases the observed backscattering coefficient (*Ulaby et al. 1986*).

The effect of vegetation on backscattering is typically very small and mainly dominated by its volumetric moisture content and the overall height and amount of vegetation (*Ulaby et al. 1986, Fung 1994*). In the boreal forest zone the amount of undergrowth and the resulting radar backscattering is typically quite small.

After the snow-melt season the ground layer is typically wet. The C-band backscattering level for wet ground is typically several decibels higher than that of wet snow. The backscattering level for wet ground is typically in the same range as dry snow (*Koskinen et al. 1997*). The difference for radar backscattering between dry snow and wet ground is neither consistent nor significant enough to allow for discrimination between them using C-band single polarization intensity imagery (*Koskinen et al. 1997*).

2.2.3 Radar backscattering from forests

The backscattering properties of forests are affected by several variable parameters. The forest type, dominant tree species and forest density are the obvious key elements, but in addition to these there are other seasonally changing and weather-dependent parameters, e.g. the volumetric moisture content of forest canopy and forest floor parameters, such as soil moisture. Additionally radar properties such as the frequency utilized and polarization affect the observed backscattering signatures.

In principle, the forest canopy increases the volume scattering contribution, and decreases the backscattering from the forest floor. One of the dominating factors is the volumetric moisture content of the canopy. Increasing canopy moisture increases the observed radar backscattering coefficient (*Ulaby et al. 1986*). The volumetric moisture content can be used to derive the permittivity and thus the backscattering properties of the canopy (*Fung 1994*). The empirical measurements conducted on Finnish boreal forest sites show the backscattering coefficient changing on the order of 2-2.5 dB as the forest stem volume ranges from 0 to 370 m^3/ha (*Pulliainen et al. 1994*). The sensitivity of C-band response to forest biomass on the boreal forest zone can be either positive or negative depending on weather and canopy conditions (*Pulliainen et al. 1996*). During the snow-melt season with wet snow conditions, the observed backscattering from forest canopy increases as stem volume increases (*Koskinen et al. 1997*).

If the effect of forest is neglected in SCA estimation, the estimates received from forested areas are biased in relation to the amount of forest stem volume of the monitored area. The backscattering contribution from forest canopy can be compensated for, if the geographical forest density distribution is known, as suggested by (*Pulliainen et al. 2001*).

2.3 Backscattering mechanisms of snow-covered terrain and their modeling

The radar backscattering signature is made up from the different contributions described in previous Sections. The overall backscattering signature can be determined by approximating the different contributions using different models and summing up the estimated contributions.

The behavior of backscattering signatures and thus its modeling is strongly influenced by the 1) frequency and 2) polarization used, and 3) the prevailing snow conditions.

The behavior of backscattering on C-band co-polarization is the main interest of this dissertation, since the operationally available spaceborne SARs function in this frequency range and polarization setup. The backscattering at lower frequencies, such as L- and S-band are less influenced by snow cover and the main contribution comes from the snow-ground interface. In the case of wet snow the contribution from the air-snow interface is the dominating factor. At higher frequencies, such as X- and Ku-band the influence of snow volume backscattering is increased, although the snow-air and snow-ground interfaces still have a large effect on the observed overall backscattering; again the snow wetness determines the overall backscattering signature and the contributions acquired from the different mechanisms. The cross-polarization measurements are mainly dominated by the volume scattering effects of the snow cover. The co-polarization measurements are more influenced by the surface scattering mechanisms. The effect of snow conditions are to a degree dependent on frequency and polarization, but in general the presence of wet snow strongly increases the snow-air interface contribution and in the case of dry snow, the contribution of snow-air interface is small, and decreases as frequency decreases.

The main contributions to the overall backscattering signature that need to be considered in the C-band, shown in Figure 2-1, are 1) direct backscattering from the snow-air interface, 2) volume scattering from the snow layer and 3) direct backscattering from the snow-ground interface, including the two-way transmissivity through the snow layer (*Ulaby et al. 1986, Fung 1994*). There are other elements that can be included in the model, such as 4) downward scattering from the snow grains followed by scattering from the ground and 5) upward scattering from the ground followed by volume scattering at the snow grains. In addition to these contributions, the backscattering is affected by multiple scattering/reflection resulting from snow volume and one or both boundaries of the snow layer.

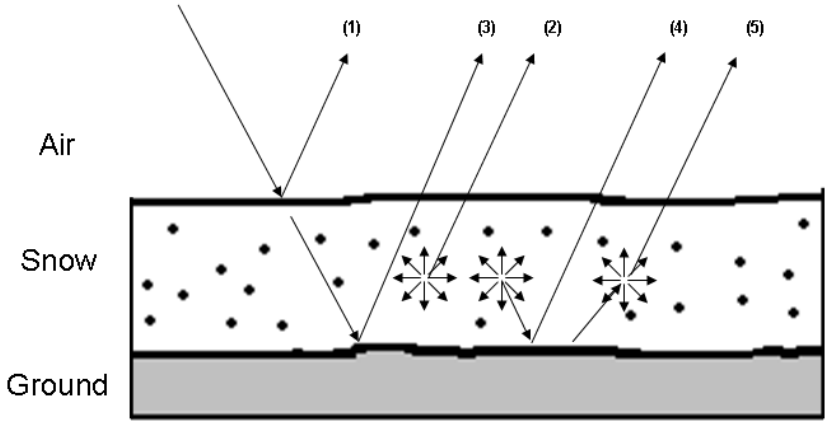

Figure 2-1. The first order scattering mechanisms (1) – (3) and some of the second order mechanism (4) – (5) illustrated for snow-covered terrain.

Typically, a relatively good approximation for C-band backscattering of snow-covered ground can be reached using the contributions (1) – (3) and the second order contributions are often neglected. The magnitude of volume backscattering (2) is typically smaller than that observed from the air-snow (1) and the snow-ground (3) interfaces. The backscattering contribution from the snow-air interface increases with

increasing snow wetness. There are a number of models that can be used to approximate the contributions (1) – (5) and some of the well established ones are briefly covered here.

There are several different surface scattering models that have been used in snow backscattering approximation, e.g. 1) Integral equation model (IEM) by (*Fung 1994*), 2) Advanced Integral Equation Model (AIEM) by (*Chen et al. 2003*) and 3) empirical Oh model by (*Oh et al. 1992*).

One of the most widely applied models, the IEM, described in (*Fung 1994*) is utilized in [P5] for modelling the backscattering from a snow-air interface. It is based on three main assumptions: 1) only single scattering is important; 2) transmission across the top boundary (air-snow interface) can be accounted for by using the Fresnel power transmission coefficient and 3) the reflection at the lower boundary for the snow-ground surface interaction can be calculated using the Fresnel power reflection coefficient. The empirical surface backscattering model for bare unfrozen soil surface presented in (*Oh et al., 1992*) is applied for a snow-ground interface in [P5]. The model is based on tower-based scatterometer measurements at L-, C- and X-band and at incidence angles from 10º to 70º.

For snow volume scattering there are also several well-established methods, e.g. 1) Dense medium radiative transfer (DMRT) model introduced by (*Tsang et al. 1985*) and 2) scattering model for snow layers. See, for example, (*Fung 1994*). The model by Fung describes the snow layer as a volume of ice particles and its utilization is investigated in [P5].

2.4 Snow-covered area estimation using radar

Snow-melt monitoring using radar is based on the variation of the backscattering signature during the seasonally changing conditions as described in previous Sections.

Discrimination of wet snow from dry snow and discrimination of snow-free ground from wet snow is feasible using C-band single polarization intensity imagery. The discrimination is based on the difference in the level of backscattering from different snow-melt conditions when a particular area is observed under sufficiently similar imaging circumstances. The discrimination of snow-covered areas from the snow free areas is in a degree challenged on the boreal forest zone by the radar backscattering induced from the forest canopy.

The capability of C-band SAR to map fractional snow-covered area is based on the decrease of backscattering coefficient with increasing snow liquid water content. This has been demonstrated using repeat pass ERS-1 SAR observations for alpine regions by (*Rott and Nagler 1993, Nagler and Rott 2000*). The method, utilizing a single reference image for SCA estimation, has also been successfully used in operational applications. It has been widely adopted for SCA estimation in mountainous regions, e.g. by (*Malnes and Guneriussen 2002*) in Scandinavia. The applicability of the method for the boreal forest zone has been investigated in [P5].

The capability of C-band SAR to map wet snow-covered areas in boreal forests is based on the decrease of the backscattering coefficient with increasing snow liquid water content. This was demonstrated, for example, by (*Baghdadi et al. 1997*) using C-band ERS-1 SAR observations for Quebec. They also proposed a wet-snow mapping procedure feasible for boreal forests when multi-temporal data are available.

Their conclusion for the applicability of HH-polarized C-band Radarsat-1 SAR observations was the same as that for VV-polarized ERS data (*Baghdadi et al., 2000*).

Similar results were reported for Finnish boreal forest and a pixel-wise SCA estimation algorithm was introduced laying the foundation for the TKK SCA method (*Koskinen et al. 1997*). The TKK algorithm employs two reference images with the same viewing geometry (representing snow-free conditions and full wet-snow cover conditions). The TKK method was further improved by including an adaptive correction factor for considering the temporal changes of forest canopy backscatter and transmissivity (*Pulliainen et al. 2001*). In this case the algorithm has to be used for larger regions than individual pixels, e.g. for drainage areas.

One of the major handicaps in the performance of wet snow mapping and SCA estimation algorithms is the influence of the surface roughness of wet snow. The algorithms work well under typical melting conditions with a smooth surface. However, if surface roughness is increased due to precipitation of liquid water or by melt-refreeze metamorphism, the level of backscatter can increase considerably, corrupting the algorithms (*Magagi et al. 2002*).

In general, the statistical accuracy characteristics of fractional snow-covered area mapping techniques are not well established. The investigations have now been carried out for the fractional snow-covered area estimation methods on boreal forest zone, and form the basis of this dissertation. The comprehensive accuracy characterizations for the method utilizing two reference images in the boreal forest zone are covered in [P1], [P2], [P3] and the characterization for the single reference image method in the boreal forest zone is presented in [P4].

2.4.1 Snow-covered area estimation using a single reference image

The snow-covered area estimation method utilizing a single reference image is presented in (*Rott and Nagler 1993, 1994*) and later refined in (*Nagler and Rott 2000*). The method utilizes the difference in backscattering coefficients when dry snow or bare ground is compared with wet snow. A reference image acquired during dry snow or bare ground conditions is required. The evaluated image is compared with the reference and if an adequate difference in backscattering coefficient is observed the investigated pixel is determined to consist of wet snow. The method is formulated as (*Nagler and Rott 2000*):

$$\begin{aligned} &\textit{if } (\sigma^{\circ}_{obs} / \sigma^{\circ}_{ref}) < TR \rightarrow (\textit{then wet snow}) \\ &\textit{else} \qquad\qquad\quad \rightarrow (\textit{then dry snow or bare ground}) \end{aligned} \tag{2-5}$$

where σ°_{obs} is the observed backscattering coefficient, σ°_{ref} is the reference backscattering coefficient from dry snow or bare ground image and TR is the threshold for snow-covered area discrimination. Using the reference image, the observed image is classified into either wet snow or bare ground/dry snow areas. When the evaluation is conducted during the snow-melt season, as is the case with these data, the classification can be determined to have only two outcomes: bare ground or wet snow (when the backscattering difference is larger than the discrimination threshold). The evaluation using equation (2.5) is carried out on a pixel level and the fractional SCA estimate for each sub-drainage basin is calculated from the binary pixel-wise snow/no-snow map.

The single reference image method was originally developed for mountainous areas, where a 3 dB threshold was determined to be an optimal threshold. Due to the different backscattering levels, different topography and environmental aspects of the boreal forest zone, an investigation was carried out to determine whether a different threshold level would be more suitable for SCA evaluation in this environment. The findings presented in (*Magagi and Bernier 2003*) further suggest that a different threshold level may be more optimal for the boreal forest zone. The results of the investigation conducted for the boreal forest zone are presented in [P4].

The single reference image SCA method discriminates wet snow-covered areas from bare ground, based on the backscattering difference between the two. The authors (*Nagler and Rott 2000*) suggest using a three decibel threshold to separate snow-covered areas from snow-free ground. A more modest threshold level is suggested by (*Magagi and Bernier 2003*). Additionally, the backscattering levels observed in the boreal forest zone, (see e.g. [P4] Table 1), suggest that a smaller threshold level may yield more accurate SCA estimates. Also the selection of reference image will probably affect the optimal level for the estimation threshold.

2.4.2 Snow-covered area estimation using two reference images

The method utilizing two reference images for SCA estimation is presented in (*Koskinen et al. 1997*). It is based on the variation of radar backscatter from snow and ground layers during the spring snow-melt season, reported in (*Stiles and Ulaby 1980, Ulaby et al. 1986, Strozzi et al. 1997*). In C-band the level of backscattering from wet snow is generally lower than that of dry snow or bare ground. The backscattering coefficient typically decreases with increasing snow wetness. As the snow-melt season progresses, the snow layer melts and the underneath bare ground is revealed. Bare ground typically has a much higher level of backscattering when compared with wet snow; so as the amount of bare ground increases, the amount of backscattering also increases. When all the snow has melted and only bare ground is visible, the backscattering level is the highest. This temporal variation on radar backscattering illustrated in Figure 2-2 is utilized for SCA evaluation.

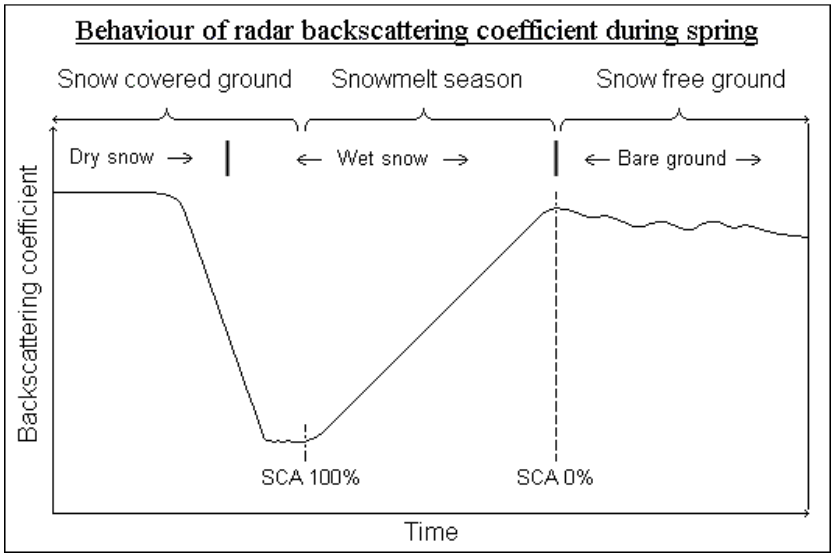

Figure 2-2. The behaviour of backscattering coefficient during the snow-melt season.

Two reference images are needed for SCA estimation. One presents the wet snow situation at the beginning of the snow-melt season, while the other describes the snow free situation at the end of the snow-melt season. The reference images define the backscattering levels for the SCA estimation, thus the acquisition instances for them have a critical effect for the estimation accuracy. The reference image for the beginning of a snow-melt season needs to be chosen so that the snow layer is wet and the ground is completely covered by snow. The backscattering coefficient of bare ground depends on the soil moisture and the state of the ground vegetation. Since these parameters vary temporally, the optimal time for the reference image acquisition for the end of snow-melt season is when all the snow has melted and the ground is still wet. The selection or acquisition of suitable reference images can be carried out using 1) traditional ground-based observation data (e.g. weather station, snow course or in-situ observation data), 2) snow maps derived from remote sensing data, 3) meteorological data or 4) the observed backscattering coefficients (which requires information of the suitable reference backscattering levels, as described in Section 3.2.2 and [P3]), or a suitable combination of the aforementioned.

The SCA estimation is carried out by a linear interpolation algorithm that uses the reference images to estimate the snow-covered area. The linear interpolation method was formulated in (*Koskinen et al. 1997*). The method is based on the assumption that the observed surface backscattering coefficient is a linear combination of the backscattering from the area covered by snow and the area of snow-free ground. If the fraction of snow-covered ground is denoted by SCA then the area of snow-free ground is (1-SCA). The observed backscattering coefficient can then be written using the backscattering levels and the fraction of snow-covered area

$$\sigma^\circ_{surf} = SCA \cdot \sigma^\circ_{snow} + (1 - SCA) \cdot \sigma^\circ_{ground} \tag{2-6}$$

where σ^o_{surf} is the total surface backscattering coefficient, σ^o_{ground} is the backscattering coefficient from the snow-free ground and σ^o_{snow} is the backscattering coefficient from the snow-covered ground. When this equation (2-6) is solved for SCA, it is seen that SCA can be solved for any evaluated image when backscattering levels for the snow-free ground and snow-covered ground are known

$$SCA = 100\% \cdot \frac{\sigma^\circ_{surf} - \sigma^\circ_{ground,\,ref}}{\sigma^\circ_{snow,\,ref} - \sigma^\circ_{ground,\,ref}} \tag{2-7}$$

where σ^o_{surf} is the observed surface backscattering coefficient, $\sigma^o_{ground,\ ref}$ is the reference backscattering coefficient from the snow-free ground and $\sigma^o_{snow,\ ref}$ is the reference backscattering coefficient from the wet snow-covered ground. With the knowledge of the reference backscattering signatures, the SCA can be solved from the observed backscattering coefficient.

The linear interpolation algorithm can be used in a pixel-wise manner, resulting in an independent SCA estimate for each image pixel. Pixel-wise SCA estimation is however impractical because of the uncertainty produced by radar speckle. Because of speckle and since the end products are typically calculated for, for example, hydrological drainage basins, the SCA estimation is typically performed for areal computational units consisting of hundreds or thousands of pixels. The SCA estimates are acquired by averaging the backscattering signatures for the pre-defined computational units (e.g. drainage basins), and evaluating the resulting SCA for them.

In addition to the linear interpolation algorithm, an adaptive algorithm for boreal forest canopy compensation for SCA estimation was suggested by (*Pulliainen et al. 2001*). A comprehensive evaluation including a quantitative characterization of the estimation accuracy for the SCA estimation and the forest canopy compensation was presented in [P1]. The linear interpolation algorithm and the forest compensation procedure form the basis of the TKK SCA estimation method, which is discussed in the following Chapters of this dissertation.

2.5 Retrieval of additional snow parameters using SAR data

Current spaceborne SARs have been shown to be feasible for snow-covered area monitoring during the spring snow-melt season, as described in the previous Section. In addition to the SCA, there are a few other snow parameters that can be monitored using SARs. Snow water equivalent (SWE) describes the thickness of the water layer that would form if the whole snow pack would be melted. Snow wetness describes the amount of liquid water that is contained within the snow.

Applicability of SAR for snow monitoring is strongly dependent on snow conditions. If an observed layer is thin and composed of dry snow, the lower the frequency the more difficult it is to evaluate the snow's composition using microwave radar. If the snow layer is dry, as it typically is during the winter or snow accumulation period, polarimetric or multi-frequency SAR including high frequency bands can be used to determine the snow water equivalent of the snow pack. Estimation of SWE can be carried out using a combination of different frequencies or different polarizations see, for example, (*Shi and Dozier 1995, Bernier et al. 1995, Shi and Dozier 2000, Shi 2006*). Snow Depth (SD) can be connected to SWE by approximating the snow density using measured or estimated data. In a similar manner, SWE can also be evaluated from SD measurements if snow density can be estimated. An algorithm applying SAR interferometry has been proposed for SD estimation by (*Guneriussen et al. 2001*).

During the spring snow-melt season, the snow layer is typically wet. Under wet snow conditions SAR cannot be used to determine SWE, but it can be utilized for SCA estimation. Additionally, SAR can be utilized in some circumstances for the determination of snow wetness. A methodology for snow wetness detection using C-band co-polarization SAR is presented in [P5].

Classification of snow status i.e. dry snow, wet snow or no snow can be carried out by combining SAR data from different frequencies. C-band SAR can be used to discriminate between dry snow and wet snow or wet snow and bare ground. X-band SAR can be used to discriminate between dry snow and bare ground, see, for example, (*Jääskeläinen 1993, Shi and Dozier 1997*). A combination of C- and X-band SAR data can therefore be used to produce snow status maps during practically all snow conditions.

Up to now spaceborne SAR instruments have been limited between L- and X-bands. In the future, if some of the envisioned satellite instruments are realized, SAR data will also become available from Ku-band. The investigations conducted using Ku-band scatterometry, although providing data on a coarser resolution when compared with SARs, have shown the feasibility of Ku-band radar in SWE, SD and onset of snow-melt estimation (*Nghiem and Tsai 2001, Hallikainen et al. 2005*).

3 ADVANCES IN SNOW MONITORING METHODOLOGIES

This Chapter summarizes the research performed in [P1]-[P6].

The starting point for analyses and methodology development of this dissertation was presented in Chapter 2. Concerning the boreal forest region the linear interpolation method for SCA retrieval had been proposed and evaluated using qualitative analyses (*Koskinen et al. 1997*). The forest canopy compensation procedure had been suggested but not proven in a comprehensive way (*Pulliainen et al. 2001*). In order to further develop, analyze and accommodate the suggested methodology for operational hydrological purposes, the forest compensation method had to be validated and the overall accuracy characterization for the method needed to be conducted. The TKK SCA method was proven and characterized using a comprehensive ERS-2 data set; the work is presented in [P1]. The accommodation of the TKK method for operationally usable wide-swath SAR data was performed using Radarsat-1 ScanSAR wide-swath data and is explained in [P2]. Further development of the TKK method for operational SCA monitoring is presented in [P3]. The evaluation of the different fractional SCA estimation methods on the boreal forest region is presented in [P4]. The evaluation of the effect of snow wetness on radar backscattering variation during the spring snow-melt season is evaluated and presented in [P5]. The design and realization of an operational fully automatic processing system for SCA estimation, based on the TKK method is presented in [P6].

3.1 Development of SCA mapping techniques for the boreal forest zone

The TKK snow-covered area estimation method, consisting of the linear interpolation algorithm and the forest compensation procedure was analyzed using a comprehensive set of ERS-2 data from the years 1997 – 2002. The investigations carried out are presented comprehensively in [P1]. The main issues of overall accuracy, the effect of forest compensation and the feasibility of multi-year reference data utilization are briefly covered here. The SCA estimation accuracy was determined in comparison with reference data acquired from the Finnish Watershed Simulation and Forecasting System (WSFS), run by Finnish Environment Institute (SYKE) (*Vehviläinen 1994*). The forest compensation procedure suggested by (*Pulliainen et al. 2001*) is briefly introduced here with the main results of [P1].

3.1.1 Compensation of forest canopy effects in SCA estimation

The radar backscattering coefficient is a sum of backscattering signatures from different sources. Some contributions are caused by the snow and ground layers, some are caused by the backscattering from forest canopy. The contribution from forest canopy is not related to the SCA and it is therefore a source of error. This error can be minimized by using the forest compensation method. The method is based on the boreal forest semi-empirical backscattering model by (*Pulliainen et al. 1994, 1996, 1999*). It has been adapted to work on both VV- and HH-polarizations in [P1] and [P2]; the calibration for the two polarizations is based on HUTSCAT scatterometer and ERS-1/2 measurements, presented in (*Pulliainen et al. 1994*) and (*Pulliainen et al. 1999*). Using this model the contribution of backscattering of forest canopy is calculated, and this contribution is reduced from the total observed backscattering coefficient. The corrected value is then used in the SCA estimation. The boreal forest

backscattering model describes the backscattering coefficient (σ^o) as a function of stem volume

$$\begin{aligned}\sigma^\circ(V,a,\theta,\sigma^\circ_{surf}) &= \sigma^\circ_{surf}\cdot\exp\left(\frac{p_1\cdot a\cdot V}{\cos\theta}\right)\\ &\quad + p_2\cdot a\cdot\cos\theta\cdot\left[1-\exp\left(\frac{p_1\cdot a\cdot V}{\cos\theta}\right)\right]\\ &\equiv \sigma^\circ_{surf}\cdot t(V,a,\theta)^2+\sigma^\circ_{can}(V,a,\theta),\end{aligned} \tag{3-1}$$

where V is the forest stem volume [m³/ha], σ^o_{surf} is the backscattering coefficient of the ground or snow layer and θ is the angle of incidence. The first term of equation (3-1) defines the backscattering contribution from a ground or snow layer σ^o_{surf} and the two-way transmissivity through the forest canopy t^2. The second term of equation (3-1), σ^o_{can}, defines the forest canopy backscattering contribution. The polarization coefficients p_1 and p_2 depend on the frequency and polarization. The values for C-band VV-polarization are $p_1 = -5.12\cdot10^{-3}$ and $p_2 = 0.131$, while for C-band HH-polarization they are $p_1 = -4.86\cdot10^{-3}$ and $p_2 = 0.099$. The variable a defines the conditions of forest canopy (related to canopy total water content and frost status) and needs to be solved for the particular weather conditions according to observed backscattering coefficients.

Using equation (3-1) the backscattering contribution for forest canopy can be determined by extracting backscattering coefficients representing different stem volume classes from the satellite images by using the forest stem volume information. The process consists of a non-linear fit of the observed backscattering coefficients to the model, where the parameters a and σ^o_{surf} are the variables to be optimized. For the optimization the backscattering for each stem volume class need to be calculated. The minimization problem is written

$$\min_{a,\sigma^\circ_{surf}} \sum_{i=1}^{n} w_i\cdot\left(\left\langle\sigma^\circ_{OBSERVED,i}\right\rangle-\sigma^\circ(V_i,a,\sigma^\circ_{surf})\right)^2, \tag{3-2}$$

where n is the number of stem volume classes, $\left\langle\sigma^\circ_{OBSERVED,i}\right\rangle$ is the mean observed backscattering coefficient for the stem volume class V_i and σ^o is the model-predicted average backscattering coefficient. The weighing factor w_i is used if the stem volume classes are unevenly distributed. When the minimization has been conducted and the parameters for the backscattering coefficient are known, the solved variables a and σ^o_{surf} can be used with equation (3-1) to calculate the backscattering coefficient without the contribution from the forest canopy, corresponding to the backscattering with stem volume of 0 m³/ha. This is the forest compensated backscattering coefficient that is used in the linear interpolation phase of SCA estimation. The basis of forest compensation is illustrated in Figure 3-1.

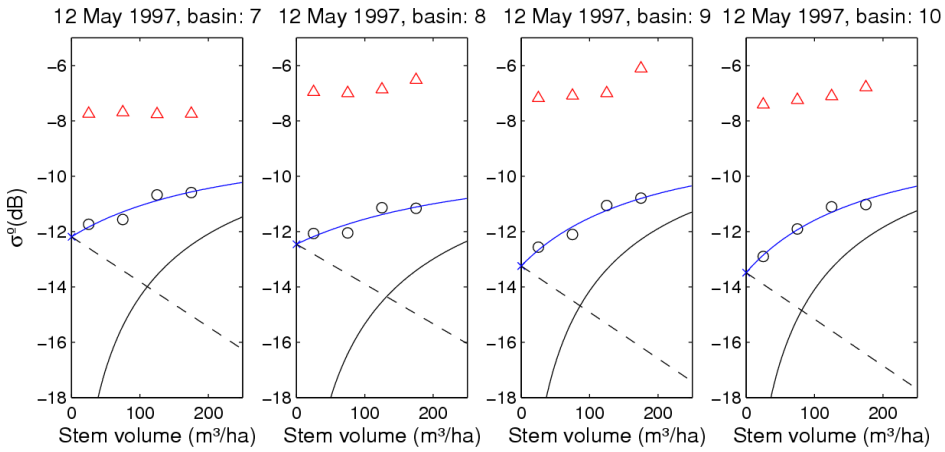

Figure 3-1. The forest compensation model visualized for the snow-melt season of 1997. The contribution from the forest canopy is drawn with the solid black line, the surface (partially snow-covered ground) contribution is drawn with a dashed black line and the total modeled backscattering coefficient is drawn with a solid blue line. The observed backscattering coefficients (ERS-2 data) are drawn with circles, and the model is fitted to these values. The forest compensated value is acquired from the point where stem volume reaches 0 m³/ha. In addition, the observations for snow free conditions of 18 May 2001 are shown using red triangles. The drainage basins of the Kemijoki region in northern Finland are labelled according to the ERS-2 investigation (Detailed information on [P1] page 2).

When both the forest compensation procedure and the linear interpolation algorithms are utilized, the SCA is estimated independently for open and forested areas. The discrimination between open and forested areas is based on the forest stem volume information of the target area (the forest classification of northern Finland is utilized throughout this dissertation, see Section 3.1.2.1). The pixels representing the open areas are averaged to produce the areal backscattering coefficient for the open areas. The pixels of the forested areas are used with the forest compensation procedure to produce the forest compensated backscattering coefficient. These values are then utilized in the linear interpolation phase, thus providing the SCA estimates for open and forested areas. A combined SCA estimate for a certain area, e.g. a drainage basin, can be calculated by weighing the different contributions based on their respective areal coverage. The SCA estimates have been designed to be readily applicable in hydrological applications, e.g. with the Finnish WSFS.

3.1.2 Characterization of the TKK SCA method using ERS-2 data

3.1.2.1 Test site, satellite data and reference data

The test site for the ERS-2 investigation is located in northern Finland and consists of 14 Kemijoki river drainage basins, having a total area of 1162 km². Representation of the test site is shown in [P1] (Figure 1). The test site represents typical northern boreal forest: relatively sparse coniferous forests, with some open areas, which are typically bogs. The topographical variations within the test area are very modest in general and the area can be described as non-mountainous. The average drainage basin size was 83 km² and was dominated by boreal forest. On average the open areas contained 18.6 % and forests covered 80.4 % of the land area. The land-use classification

discriminates the forested areas according to stem volume classes (0-50, 50-100, 100-150, 150-200 and over 200 m³/ha). The land-use classification data have been produced by the National Land Survey of Finland. The data are based on the National Forest Inventory of the Finnish Forest Research Institute. The Forest Inventory data are based on cartographic data, ground truth sampling and Landsat TM imagery (*Paavilainen et al. 1992*).

The satellite data consisted of 24 ERS-2 C-band SAR intensity images gathered during the snow-melt seasons of the years 1997, 1998, 2000, 2001 and 2002. The images are listed in [P1] (Table II). The images for the years 1997 and 1998 were rectified and geocoded using software developed at the Technical Research Centre of Finland (VTT). The software uses the Rauste algorithm (*Rauste 1989*), which employs a digital elevation model (DEM) to correct errors caused by topography. The images from the years 2000, 2001 and 2002 were processed using Gamma Ltd. Software (*Wegmüller et al. 1998*).

All ERS-2 PRI images were processed using the DEM resolution of 25 m, and thereafter the images were sampled into the spatial resolution of 100 m. Of the 24 images, 5 represented the snow conditions of a wet snow with SCA near 100% and were candidates as the reference images for the beginning of snow-melt season. 7 images represented the situation with SCA near 0% and wet ground, and were chosen as reference image candidates for the end of snow-melt season. The other 12 images represented the situation during the snow-melt season with SCA between 0% and 100%. The SCA was estimated also for the reference images.

The SCA estimation results were compared with data from simulations of the operational hydrological model WSFS. WSFS simulates the hydrological cycle for all the land area of Finland daily (*Vehviläinen 1994*). Forecasts for river discharge and water levels are made for 5500 drainage basins, to which the fourteen basins used in this study also belong.

The WSFS is managed by the Finnish Environment Institute's Hydrological services division, and according to their analyses the WSFS SCA has been shown to have a root-mean-square error (RMSE) of 20% units on average and the SCA estimates are non-biased (Huttunen 2004). The WSFS data include daily SCA information for all the 14 drainage basins; separate values are shown for the open and the forested areas.

3.1.2.2 The overall statistical accuracy for narrow-swath SAR data

The main goal for the ERS-2 analyses, presented in [P1], was the assessment of the overall accuracy and the analysis for the forest compensation procedure.

The first step of the analysis was to determine the overall accuracy of the SCA estimation. Since there were 5x7 different reference image combinations (5 reference images of wet snow, 7 reference images of bare ground), there were also performance variations between the different reference image pairs. Thus an average accuracy of all the reference image combinations can be viewed as the average performance of the method. The results that were acquired with the best reference image pair can be interpreted as the accuracy when the reference image selection succeeds. There were 7280 SCA estimates for different reference image combinations for both open and forested areas and 268 estimates for the best reference image pair. The results of the analyses are shown in Table 3-1.

Table 3-1. The overall accuracy analysis for the baseline TKK SCA method using ERS-2 data from 1997, 1998, 2000, 2001 and 2002.

	Open areas		**Forested areas**	
	All combinations	Best pair	All combinations	Best pair
RMSE	0.282	0.213	0.207	0.179
Mean abs. error	0.209	0.137	0.154	0.119
Bias	+0.180	+0.095	+0.043	-0.049
Correlation coefficient	0.830	0.873	0.860	0.896

The results show that the differences between the average accuracy obtained with all the reference image combinations and the accuracy obtained with the best reference image pair are quite considerable. The higher performance obtained with best reference image pair is remarkable in all aspects of the statistical accuracy analysis.

The RMSE is improved by 24 % in the case of open areas, and 14 % in the case of forested areas. The improvement in mean absolute error is 34 % for open areas and 23 % for forested areas. The bias is improved by 47 % for open areas, but slightly weakened for forested areas. The linear correlation coefficients are also clearly improved in the case of the best reference image pair. These are visualized by plotting the estimated SCA with respect to the reference SCA values in Figure 3-2.

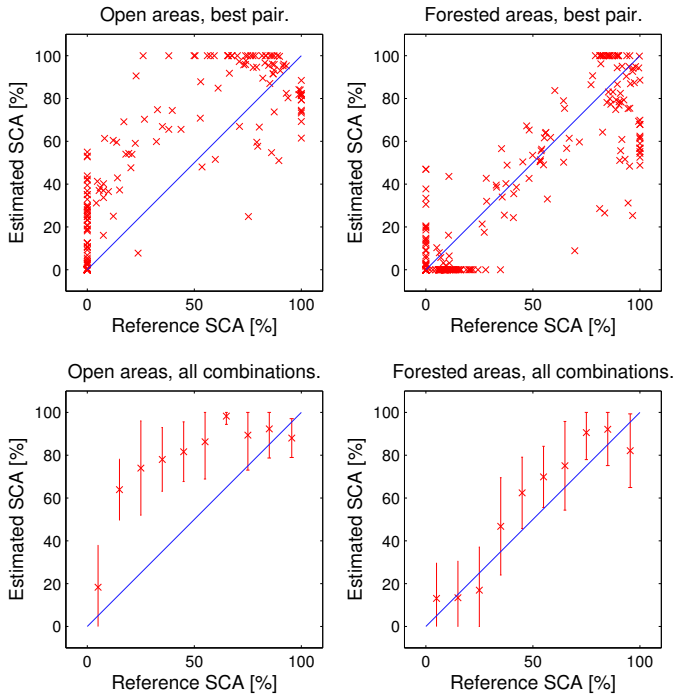

Figure 3-2. The ERS-2 derived SCA estimates plotted in comparison with reference SCA values for the cases of best reference image pair (above) and the cases of all reference image combinations (below). For all the reference image combinations, the number of samples were 7280, thus the graph shows the average SCA estimate and the standard deviation of the samples.

In addition to the overall accuracy analysis the performance of the method was analyzed by measuring the average RMSE for different SCA situations during the snow-melt seasons. The estimation accuracy for forested areas was quite independent of the prevailing SCA situation. However, the estimation accuracy for the open areas varied more with respect to the snow conditions. These observations can also be made from Figure 3-2.

3.1.2.3 The significance of the forest compensation

Forest compensation is a key element of the TKK SCA method. Its purpose is to minimize the effect of forest canopy backscattering in order to increase the SCA estimation accuracy. The results of the statistical analysis for forest compensation using the ERS-2 data set, presented in [P1], are shown in Table 3-2.

The results indicate that the forest compensation improves the SCA estimation accuracy. The improvement is seen in all statistical variables except the bias. The RMSE and the correlation coefficient show the highest improvement. The statistical significances of the improvements were tested using a chi-squared test. The improvements were statistically significant with 99.9% confidence interval for all the cases, and 97.5% interval for the best reference image pair. As a conclusion, the forest compensation can be considered successful and a beneficial addition to the SCA estimation method.

Table 3-2. The significance of the forest compensation algorithm, analyses carried out using the ERS-2 derived SCA data set

	All combinations		**Best ref. image pair**	
	No forest compensation	Forest compensation	No forest compensation	Forest compensation
RMSE	0.217	0.207	0.195	0.179
Mean abs. error	0.159	0.154	0.132	0.119
Bias	+0.039	+0.043	-0.038	-0.049
Correlation coefficient	0.841	0.860	0.871	0.896

3.1.2.4 Visual interpretation of SCA estimation using ERS-2 data

A visualization of SCA estimation is presented in Figure 3-3. The SCA map presents the situation for 28 May 1997 for open areas; the estimation is drawn on top of the ERS-2 SAR PRI image. This image is acquired in the middle of the snow-melt season, so a noticeable variation of SCA is seen within the image. The variation of the intensity of radar backscatter can also be noted in the image background. The backscattering near the drainage basins with high SCA on the east is weaker and the backscattering in the west where SCA is closer to zero is stronger. This is the fundamental behavior of backscattering during the snow-melt season, which was also explained by Figure 2-2.

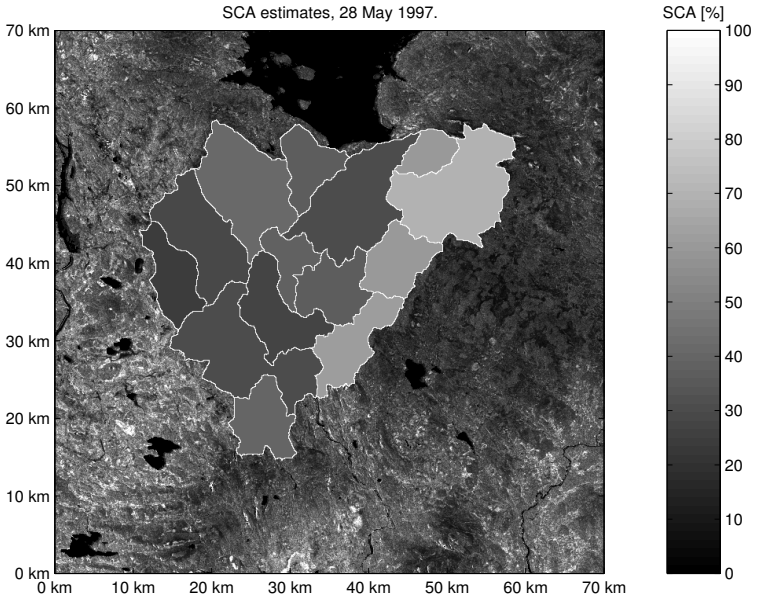

Figure 3-3. The SCA estimation visualized for 28 May 1997 using ERS-2 data. The estimates shown are for the open areas of each drainage basin (each drainage basin consist of both open and forested areas).

3.1.3 Characterization of the TKK SCA method using wide-swath SAR data

The main purpose of the Radarsat-1 SCW investigation was to establish the feasibility and the accuracy of operational SCA estimation when wide-swath SAR images are used. The investigations conducted are published in [P2] and [P3]. The investigations concerning wide-swath data presented within this dissertation have all been carried out using Radarsat-1 data. All available data from the melt seasons of 2004, 2005 and 2006 have been utilized here, as in [P3]. The investigations presented in [P2] included only data from the years 2004 and 2005.

3.1.3.1 Test site, satellite data and reference data

Analogously to the case of narrow-swath SAR-images, the operational feasibility of the TKK SCA estimation method for wide-swath SAR-data was studied using Northern Finland as the test area. The area is similar to the one used in ERS-2 investigation, although significantly larger. The test region utilized is bound by the Finnish state borders and spans between 65° and 70° northern latitude (geographical location of the area is shown in Figure 1 of [P3]). The investigation was carried out using the drainage basin classification. A typical drainage basin in Northern-Finland has a size between 10 and 100 km² with an average size of 74.9 km². The landscape of Northern Finland is non-mountainous and the topographical variations throughout the test area are quite modest. The studies were carried out in a manner similar to the ERS-2 investigation, combining the open areas and the open bogs as one category; and combining the forested areas and forested bogs for another category. On average the amount of open areas was 50 % and forest covered 43 % of the total area. The water surfaces (7% of total area) were excluded from the analyses.

The satellite data consisted of 14 Radarsat-1 C-band SAR intensity images from the snow-melt seasons of 2004, 2005 and 2006. All the images were from ascending node. The imaging mode used was ScanSAR Wide A (SCW), which provides an

operationally suitable 500 km swath width. Radarsat-1 employs HH-polarization and the satellite data used are listed in Table 3-3.

The difference in the incidence angles between the reference and evaluated images might be a concern if the difference becomes too large. With these data, the largest difference was 12.8°. This is already a significant difference; however, the results indicate that it does not hinder the SCA estimation. It is also worth noting that in forested areas the influence of incidence angle is reduced by the forest compensation algorithm (see equation (3-1)).

Table 3-3. The Radarsat-1 SCW dataset utilized in the analyses. The incidence angle value is from a central drainage basin of northern Finland.

Date	Incidence angle for centre	Progress of snow melt season
18 April 2004	30.8°	Beginning of melt season
28 April 2004	36.2°	Middle of melt season
5 May 2004	33.9°	Middle of melt season
12 May 2004	31.7°	Middle of melt season
26 May 2004	25.7°	End of melt season
30 March 2005	36.1°	No snow melt (dry snow)
30 April 2005	33.6°	Beginning of melt season
7 May 2005	30.9°	Beginning of melt season
14 May 2005	28.1°	Middle of melt season
31 May 2005	30.9°	End of melt season
2 May 2006	30.9°	Beginning of melt season
5 May 2006	38.5°	Middle of melt season
9 May 2006	28.1°	End of melt season
12 May 2006	36.1°	End of melt season

The Radarsat-1 SCW images were rectified and processed using the orbital parameters and calibration information acquired from the satellite data provider Kongsberg Satellite Services AS (KSAT) and a TKK-developed rectification program (*Kärnä et al. 2005*). The image of 18 April 2004 represented the snow conditions for wet snow with SCA near 100% and was chosen as the reference image for the beginning of the snow-melt season. The image of 26 May 2004 represented the situation with SCA near 0% and wet ground, and was chosen as the reference image for the end of the snow-melt season. These reference image selections apply to the baseline method evaluated in Section 3.1.3. The images labeled with "Beginning…", "Middle…" or "End of snow-melt season" were all utilized in the accuracy analyses. The images with labels "Beginning…" or "End of melt season" were additionally candidates for the enhanced reference image selection procedure, described in Section 3.2.2., which means that for some parts of the images the snow conditions were applicable to be used as reference; i.e. the overall snow-melt season was either at early or late stages.

The performance of radar-based SCA estimation was evaluated by comparing the radar data-derived SCA estimates with SCA estimates determined from optical satellite data. The Finnish Environment Institute (SYKE) has been monitoring SCA in Finland during snow-melt seasons with data acquired from the NOAA/AVHRR and the Terra/MODIS instruments (*Metsämäki et al. 2002, 2005*). The SCA values applied here covering the years 2004-2006 were processed from Terra/MODIS observations,

as MODIS data have been shown to produce more accurate SCA estimates than AVHRR data for the boreal forest zone (*Eskelinen et al. 2008*).

The optical SCA method has been developed and adjusted to perform optimally on the northern boreal forest zone, main emphasis being on the land areas of Finland. The method has been applied in operational use since 2001. The statistical accuracy of the optical method has been well established for Finland, using multi-year observations and multiple data sources (*Metsämäki et al. 2002, 2005*). The SCA derived by optical remote sensing method has been shown to have a RMSE of 10%-units on average using Terra/MODIS data. The reported analyses also clearly indicate that the optical SCA estimates are non-biased.

Since cloud cover and illumination conditions are limiting factors when using the optical EO-data, there can be long time gaps in the exploitable data during the snow-melt season. In the comparison work this means that the available optical SCA data and the radar-based SCA data do not necessarily coincide, so a small temporal separation was allowed for the data analyses. The magnitude of temporal separation for each reference value was also noted, so that results acquired with different temporal separations could be evaluated. The main analyses were conducted using a maximum separation of two days for the compared data sources.

The optical SCA method does not distinguish the SCA estimates between open and forested areas; a single estimate presents the condition of a single drainage basin. Consequently evaluations were carried out for the combined estimate representing both open and forested areas in the drainage basin under investigation.

3.1.3.2 The effect of incidence angle variation on SCA estimation

The main difficulty in the wide-swath data is the largely varying incidence angle within the SAR image. The incidence angle in SCW data varies between 20° and 49°. Since the radar backscattering coefficient is significantly affected by the incidence angle, it was essential to determine whether successful SCA estimation was possible with the wide-swath data.

The effect of the incidence angle variation was investigated by evaluating the average RMSEs of the SCA estimates for different incidence angle intervals. A 1° interval was used in the analysis. The TKK method produces SCA estimates for open and forested areas independently, while the optical data-based reference SCA shows a combined value for each drainage basin. Therefore, a combined (open + forest) SAR-based SCA estimate was calculated for each drainage basin for the analyses.

The average RMSEs and the standard deviations for the different incidence intervals are plotted in Figure 3-4. The interpretation of the plot is quite obvious; there is a decent variation of SCA estimation accuracy on different intervals, but the incidence angle does not determine, nor correlate with the SCA estimation accuracy. The key issue concerning the wide-swath SAR utilization for operational SCA estimation is therefore resolved.

There are two essential factors that need to be considered for these results. All the acquired SAR images were taken in ascending node, so the change of incidence angle occurs in the same direction within the images. The second issue was the fact that the images were intentionally selected to maximize the coverage of Northern-Finland. Therefore the different images had less than 12.8° difference in their respective

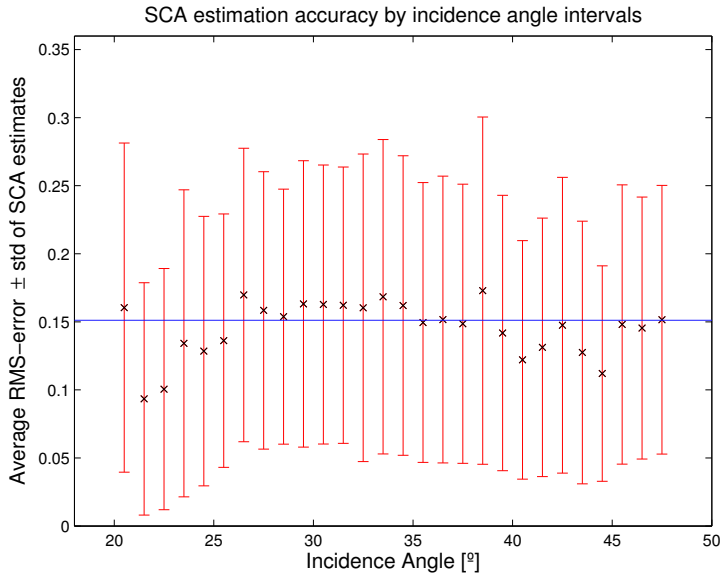

Figure 3-4. The average RMS error of Radarsat-1 SCW-derived SCA estimates in comparison with the average incidence angles of the corresponding drainage basins. The blue line represents the average RMS error of all the samples.

incidence angles. These two factors are likely to be relevant for the successful utilization of the wide-swath imagery.

3.1.3.3 The overall statistical accuracy for wide-swath SAR data

The overall statistical accuracy was investigated by comparing the SAR-based SCA estimates with the optical reference data. The statistical accuracy was determined for the different snow-melt seasons separately and an analysis for the complete dataset was also performed. The analyses were made for the combined SCA estimates (open + forested areas). The temporal difference between the estimated and the reference data is considered in the following Sections. For the baseline dataset, a maximum temporal separation of two days between the reference and estimated data was used. The results for the analyses are shown on Table 3-4.

Table 3-4. The overall accuracy analysis for the TKK SCA method using Radarsat-1 SCW data.

	Yearly datasets			**Complete dataset**
	2004	**2005**	**2006**	
RMSE	0.128	0.172	0.156	0.151
Mean abs. error	0.087	0.120	0.116	0.108
Bias	0.008	-0.064	-0.015	-0.017
Correlation coefficient	0.933	0.884	0.800	0.914
No. of samples	2772	1628	4620	9020

The results show extremely good performance for the complete dataset. The RMSE is of the same order of magnitude as the established accuracy of the reference data. The

biases are very low and the correlation coefficients are high. The number of samples, meaning the number of analyzed drainage basins, is several thousands for all years, and the size of the complete dataset is 9020 samples. The results for the snow-melt season of 2004 are slightly better than those of 2005 and 2006. When these results are compared to the results acquired in the ERS-2 investigation, it is seen that the results with Radarsat-1 SCW data are clearly better. One of the main concerns about the utilization of the SAR-based SCA estimation operationally is the overall bias of the SCA estimates. According to these analyses the bias is very low.

3.1.3.4 Temporal aspects concerning the wide-swath SAR-based SCA estimation

Several issues concerning the temporal aspects of the SCA estimation were studied. The first aspect is the temporal difference between the optical reference and the Radarsat-1 SCA data. This was studied by varying the maximum allowed temporal separation between the two data, and analyzing the results. The results shown on Table 3-5 indicate that a small difference in the allowed separation of the data does not change the outcome significantly. The best results were acquired with temporal separation of only 1 day, but using 2 days as the baseline, there were more samples for the overall analyses, and the accuracy acquired is still very good. The results from the larger temporal separations were slightly different than in [P2]. The difference is due to the fact that the large number of samples from 2006 had a significant effect on the overall analyses and for these investigations, the NOAA/AVHRR data were not utilized, as they are less accurate than the MODIS based comparison data.

Table 3-5. The effect of temporal separation between the Radarsat-1 SCW based and optical reference SCA data. (Complete dataset of 2004, 2005 and 2006)

Separation days (max)	RMSE	Bias	Correlation coefficient	Samples	RMSE without forest compensation
0	0.150	-0.045	0.923	5046	0.157
1	0.144	-0.030	0.919	7578	0.149
2	0.151	-0.017	0.914	9020	0.156
3	0.153	-0.020	0.913	9198	0.161
4	0.148	-0.020	0.925	10308	0.155
5	0.151	-0.0214	0.922	10703	0.160

The second aspect was related to utilization of multi-year reference data, which was shown to be feasible with ERS-2 data, and was now considered for the wide-swath imagery. Both reference images for this study were acquired during the year 2004. The SCA estimation seems to succeed very well also for the years 2005 and 2006, using the reference data from year 2004. The slightly inferior estimation accuracy is not large enough to draw a conclusion against the use of multi-year reference imagery.

3.1.3.5 The significance of forest compensation for wide-swath SAR SCA estimation

Forest compensation is an essential element of the TKK SCA estimation method. The benefit of the algorithm was established using ERS-2 data in [P1]. The influence of

forest compensation for wide-swath SAR data was investigated by comparing the results of the TKK method to the results of SCA estimation without the forest compensation algorithm. The results of these investigations agree with the ERS-2 findings. The RMSE, bias and mean absolute error increased and the correlation coefficient decreased when the forest compensation algorithm was not applied. The RMSE without forest compensation was 0.156 for the baseline dataset of 9020 samples, and 0.151 using the compensation, respectively. The improvement of forest compensation was found to be statistically significant with 99.9% confidence interval, when examined by a chi-squared test. An investigation concerning the temporal difference in reference data was also conducted for the forest compensation. The results are shown in Table 3-5. It is obvious in all cases that the forest compensation increases the SCA estimation accuracy.

3.1.3.6 Visualization of SCA estimation using Radarsat-1 data

A visual interpretation of SCA estimation is shown in Figure 3-6. It shows the SCA estimates acquired with Radarsat-1 SCW and Terra/MODIS data. The SCA maps present the situations for 5 May 2004 and 6 May 2004 for combined (open + forests) areas. Even as this particular image has one of the best conditions of all the optical images, the hindrance of cloud cover is seen as some patchy areas with no data. The agreement between the optical and radar-based SCA map is apparent. The snow-melt situations are quite typical for northern-Finland, the southwestern parts, near the Gulf of Bothnia reach snow free conditions first, while high lands in Northern-Lapland are still partially snow-covered.

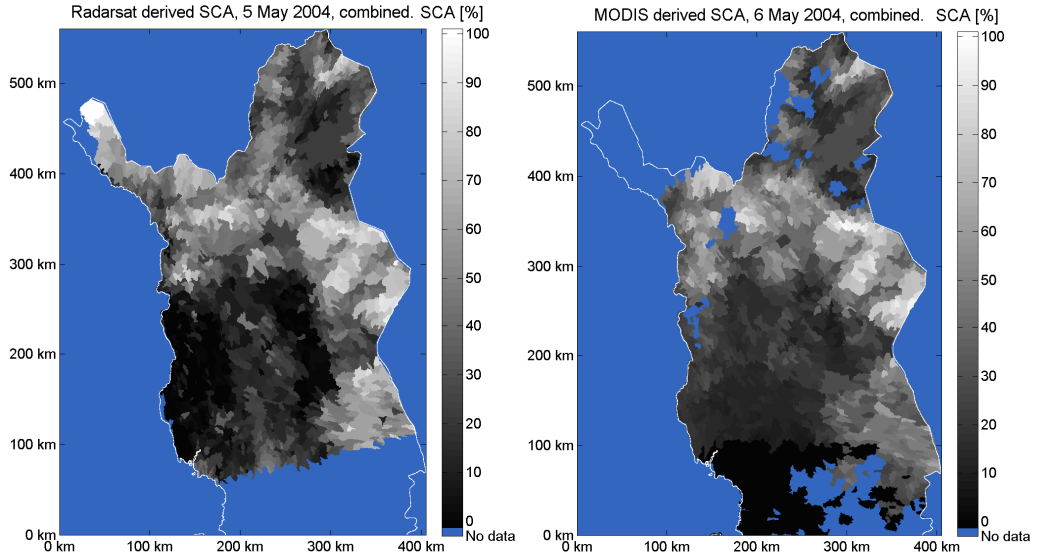

Figure 3-6. The SCA estimation visualized for radar- and optical-based satellite imagery. The Radarsat-1 SCW-based visualization on the left-hand side is for 5 May 2004 and the optical presentation on the right-hand side is for 6 May 2004. The estimates are shown for combined open and forested areas.

3.1.4 Conclusions for the baseline TKK SCA estimation method

The ERS-2 investigation, published in [P1], established the statistical accuracy of the TKK SCA estimation method. It proved the benefits of the forest compensation

algorithm and validated the utilization of multi-year reference data. The Radarsat-1 investigation, presented in [P2] and [P3], shows that the SCA estimation can be carried out in the boreal forest zone using wide-swath SAR data. The independence of estimation accuracy from the largely varying incidence angle was also proven. The statistical accuracy characterization shows very good results for the TKK SCA estimation method. The results of the forest compensation algorithm support the prior findings from the ERS-2 investigation [P1]. The TKK method was found to be well suited for operational SCA estimation.

3.2 Development of the enhanced TKK SCA estimation method

The development of the enhanced TKK SCA estimation method is presented in [P3]. The enhanced TKK SCA estimation adds two new features to the baseline TKK method. The first feature, a weather station assimilation method, utilizes ground-based observation data to improve estimation accuracy at the end of the snow-melt season. The second feature enhances the SCA estimation accuracy through a new computational scale reference image selection procedure. The new method is evaluated with respect to both additions and the overall accuracy of the enhanced method is determined. The test area, satellite data and the reference data are similar to the previous Radarsat-1 investigation, presented in Section 3.1.3.

3.2.1 Weather station assimilation method

Snow-covered area estimation is based on the difference of the observed backscattering coefficient between wet snow and wet (bare) ground; therefore it only functions properly during the snow-melt season. If the SCA estimation method is applied after the snow-melt season is over, the basic procedure does not produce valid SCA estimates. This is caused by the fact that after the snow-melt season ends, the ground typically dries and the backscattering signature of dry ground is in the same range as that of partially snow-covered ground. Therefore, applying the SCA estimation procedure after the snow-melt season may show non-zero SCA estimates. The weather station assimilation method utilizes ground-based weather station data to determine whether the snow-melt season is actually finished and prevents the formation of the possible false SCA estimates that would be seen for post melt-season observations.

The weather station assimilation procedure compares the nominal SCA estimates with previously confirmed snow conditions (previous SCA estimates). If the comparison shows increased SCA estimates, weather station data are analysed. The spatially and temporally sparse weather station data are interpolated to cover the investigated time and area. The temporal analysis is carried out between the current satellite data instance and the previous known SCA estimates. If the weather station data do not show snow accumulation and the SCA estimates do show increased values then the SAR-based SCA estimates are corrected to indicate snow-free conditions. If the weather station data show snow accumulation between the last known and the new SCA estimates (with increased SCA estimates) or decreased SCA estimates from the previous conditions, the new estimates are approved. A generalized diagram of the assimilation procedure is shown in Figure 3-7. The spatial interpolation is carried out using the nearest neighbour method, meaning that the ground-based data is utilized from the nearest available weather station for each time step. The method has been

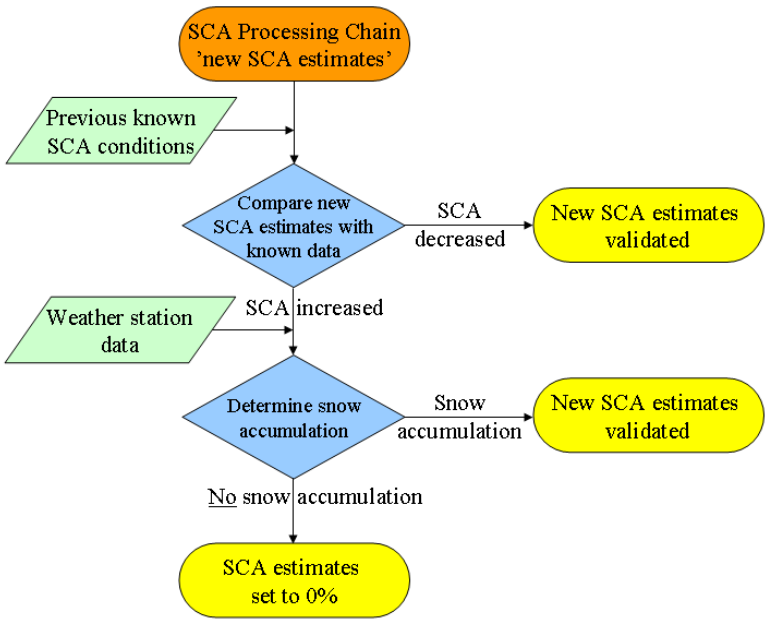

Figure 3-7. A diagram showing the weather station assimilation procedure.

designed to function as an operational system, and it evaluates the weather station data as they will be operationally available, accounting for missing or inadequate data.

3.2.1.1 The effect of weather station data assimilation

The accuracy of the weather station assimilation procedure was investigated by comparing the SCA estimation accuracy for both the new assimilation procedure and for the baseline method that excludes the use of weather station data (see Section 3.1.3). The accuracies of the two methods were compared in order to investigate if an accuracy improvement is obtained through the use of weather station data assimilation procedure.

Table 3-6. The accuracy of SCA estimation with and without weather station assimilation. Analyses were carried out by comparing Radarsat-1 SCW-based estimates with optical comparison data.

	Weather station assimilation disabled	Weather station assimilation enabled
RMSE	0.151	0.140
Mean absolute error	0.108	0.100
Bias	-0.017	-0.040
Correlation coefficient	0.914	0.934
Samples	9020	

The results of the accuracy analyses shown in Table 3-6 are convincing. The RMSE decreases notably and the overall correlation between the estimated and comparison data increases when the assimilation technique is applied. Since the majority of SCA estimates are not affected by the weather station observations (only those estimates which are suspected to be poor are affected), the overall accuracy does not change more dramatically in Table 3-6. To further evaluate the effect of the weather station assimilation, SCA estimates that did change their value due to the assimilation procedure were investigated separately (922 cases out of the 9020 samples). These results are presented in the histogram of Figure 3-8.

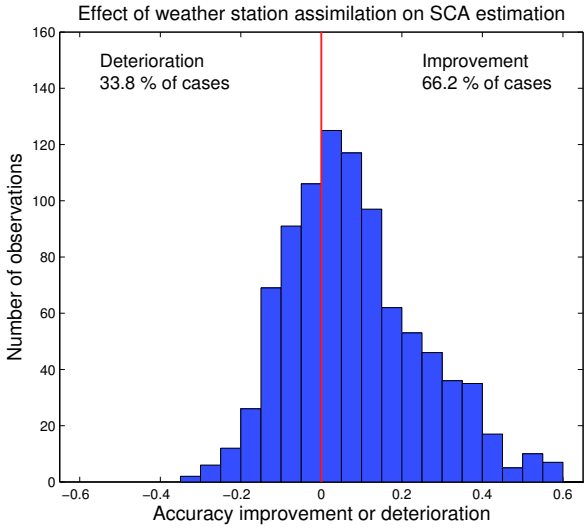

Figure 3-8. Histogram showing improvement/deterioration of SCA estimation accuracy, as weather station data are assimilated with radar-based SCA method. The 922 estimates affected by the weather station assimilation method are shown here. Analyses were carried out using Radarsat-1 SCW data.

The results show that two-thirds of the weather station assimilated SCA estimates are more accurate than the old baseline estimates. Figure 3-8 also shows that the deterioration of accuracy is in most cases very small; most samples are deteriorated less than 0.15 (values of SCA are ranging from 0 to 1). The accuracy improvement gained in most cases is notably larger. The average improvement and deterioration are 0.17 and -0.09, respectively.

Unfortunately, optical comparison data applied in the analyses were not available for all cases of radar-based SCA retrieval. The need for weather station assimilation is highlighted by the image of 12 May 2006. The SCA estimates by the original baseline method show large SCA values throughout northern Finland, as seen in Figure 3-9. However, according to comprehensive weather station data, common knowledge, and MODIS-derived SCA estimates (for 260 drainage basins), almost all of northern Finland was snow-free. The explanation for the false SCA estimates was simple: the snow-melt season had occurred and ground was snow-free and already drying. Thus, the backscattering coefficient from dry ground was lower than that of wet ground. The low backscattering coefficient was interpreted as snow-covered ground by the baseline SCA estimation method. However, previous SCA estimates from 9 May 2006 had shown very low values, and the weather station data showed no snow accumulation between the 9 May and 12 May. These are clear indications of the end

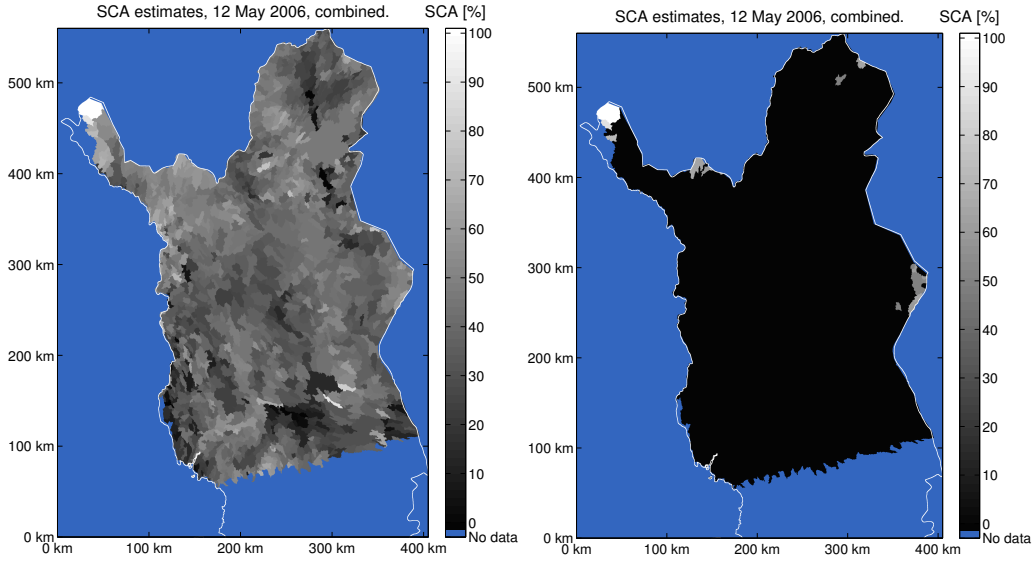

Figure 3-9. On the left hand side, the SCA estimates for 12 May 2006 acquired with the baseline SCA estimation method and Radarsat-1 SCW data. The evaluation shows high SCA values, although the actual snow conditions were snow-free. Each gray shaded area presents a different drainage basin. On the right hand side, the SCA estimates acquired with the weather station assimilation method. The evaluation shows snow-free conditions for practically all drainage basins of northern-Finland. The actual (ground truth) snow conditions were snow-free.

of the snow-melt season. The new enhanced method was designed to overcome this evident problem of the original baseline method.

Although there was a limited amount of optical comparison data available for 12 May 2006 (260 samples from 2037 drainage basins), they and the available ground truth (weather station data) indicate that practically all of northern Finland was snow-free. The SCA estimates acquired with the new enhanced method are shown in Figure 3-9. A significant improvement was achieved, as now the SCA estimates show snow-free conditions for practically all of northern Finland.

Obtained results indicate that the weather station assimilation method functions as expected close to and after the end of the snow-melt season. Furthermore, although some cases do deteriorate, the overall SCA estimation accuracy does not decrease even if the method is applied throughout the melting season. It can be concluded that weather station assimilation is a significant improvement to the baseline TKK SCA estimation method.

3.2.2 Optimization of the reference image selection process

One central aspect of the TKK method is the utilization of two reference images for the SCA estimation, providing the necessary backscattering coefficients to be used in the linear interpolation. One image represents the wet snow situation in the beginning of the snow-melt season, while the other features the snow-free situation at the end of the melt-season. When the SCA estimation is conducted for a large or a diversified area, a single image seldom represents the required conditions throughout the scene. This is the case when using Radarsat-1 SCW imagery (500 x 500 km spatial

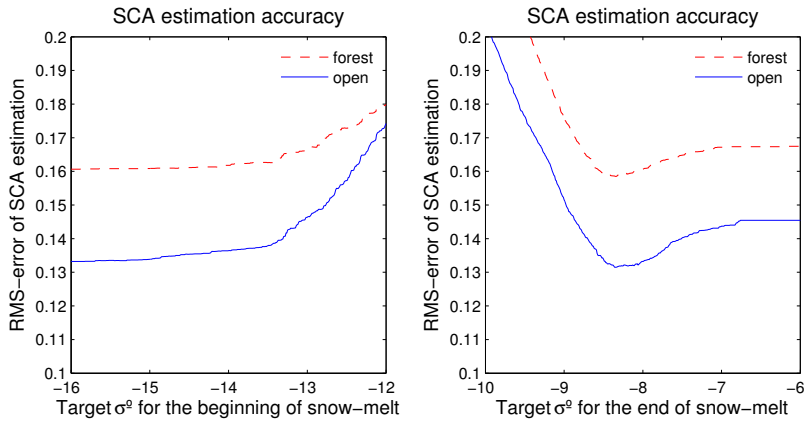

Figure 3-10. The SCA estimation accuracy shown for different target backscattering levels of reference data. The SAR data are from Radarsat-1. The reference data selection is done by choosing the closest match to the target level for both beginning and end of the snow-melt season. The selection is done independently for each drainage basin. The solid blue line shows the accuracy for open areas and dashed red line shows the accuracy for the forests; both the beginning and the end of the snow-melt season are illustrated.

coverage) for northern Finland, typically featuring different snow-melt conditions for the northern and southern parts of the image. The solution to this problem is selection of the reference images on a drainage basin level. The reference backscattering coefficients for each drainage basin are selected independently, based on the available weather station and backscattering data.

The reference image selection is carried out using the images that have been acquired near the suitable reference conditions (explained in Section 2.5). The image that has the backscattering coefficient closest to a pre-determined target value is chosen as the reference for each drainage basin. Open areas and forests are considered independently. The optimal target backscattering levels were determined in the investigations [P3], and are shown in Figure 3-10.

The optimal level for the beginning of the snow-melt season (using Radarsat-1 HH-polarized C-band data) was below -13.5dB for forests and below -15dB for open areas. The optimal level for the end of snow-melt season was between -8.5 and -8.0 dB for both open and forested areas. By using the enhanced method and the identified backscattering levels it is also easier to increase the spatial coverage of the monitored area. Spatial coverage can be expanded by adding new images with different areal coverage and finding the applicable reference data using the observed backscattering coefficients. The SCA estimation accuracy obtained with the new reference image selection method (without the weather station assimilation) is listed on Table 3-7.

It is evident from Table 3-7 that the SCA estimation accuracy is increased. The RMSE decreases, the bias are reduced and the correlation between the estimated and comparison data are improved. In addition to the increased estimation accuracy, the method is relatively easy to implement. However, it needs to be stressed that the backscattering ranges depend on the instrument, the frequency and polarization utilized and evidently also on the geographical and environmental details of the monitored area in question. Although the backscattering ranges may differ, the method itself is easily modified for other instruments and regions.

Table 3-7. The accuracy of SCA estimation using optimized reference image selection for individual drainage basins. Analyses were carried out by comparing Radarsat-1 SCW-based SCA estimates with optical reference data.

	Baseline method: Single images selected as reference	Individual reference images selected for each drainage basin
RMSE	0.151	0.136
Mean absolute error	0.108	0.096
Bias	-0.017	-0.003
Correlation coefficient	0.914	0.929
Samples	9020	

3.2.3 Overall accuracy of the enhanced TKK SCA estimation method

The overall accuracy of the enhanced TKK SCA estimation method was analyzed using the MODIS-based optical comparison data for the complete Radarsat-1 dataset. The results were compared with the accuracy of the baseline TKK method. The results for both methods are listed in Table 3-8.

Table 3-8. The accuracy of the enhanced SCA estimation method compared with the baseline TKK method. Analyses were carried out by comparing Radarsat-1 SCW-based estimates with optical reference data.

	Baseline TKK SCA method	Enhanced TKK SCA method
RMSE	0.151	0.123
Mean absolute error	0.108	0.087
Bias	-0.017	-0.003
Correlation coefficient	0.914	0.947
Samples	9020	

According to the results a significant increase in the SCA estimation accuracy is achieved. The accuracy also improved notably when compared with either the weather station assimilation or the reference image selection applied alone. According to Table 3-8, the RMSE of the estimated SCA and the comparison SCA values decreases from 0.151 to 0.123, nearly 20%, and the correlation coefficient increases from 0.914 to 0.947. The results are further high-lighted by the fact that the large dataset includes data from three snow-melt seasons (with a total of 9020 samples) and the snow-covered area estimates are acquired from all prevailing conditions during the snow-melt season. The accuracy of the enhanced method for different SCA intervals is shown in Figure 3-11. The low level of biases and the agreement between the estimated and comparison data is well portrayed.

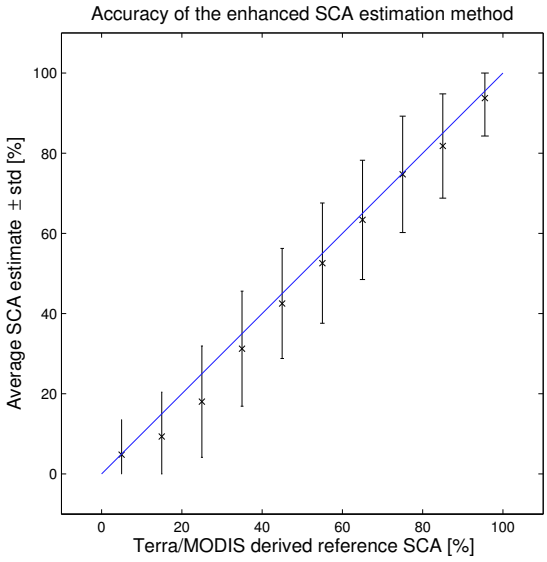

Figure 3-11. Average SCA estimates and standard deviations plotted for different SCA intervals. The intervals were determined according to the optical comparison data. A reference-line with zero error is drawn on solid blue. The analyses are shown for the enhanced SCA estimation method with 9020 samples. Analyses were carried out using Radarsat-1 SCW-based data from years 2004, 2005 and 2006.

3.3 Development of methods for operational SCA estimation for boreal forest zone

The key motivation for the development of the SCA estimation method was to create a methodology that could be utilized in operational use. The work that has enabled the operational implementation of the TKK SCA estimation method is presented in [P2] and [P6]. The intended end-users for the methodology included the hydrologists who forecast the river discharge volumes and the water reservoirs during the snow-melt season. For the hydropower industry, accurate knowledge of the snow-cover and thus the amount of water that is still available upstream from the hydropower facilities, is extremely important and valuable information that can be used to prevent floods and to optimize the hydropower operations. The knowledge of the SCA could be utilized in the hydrological forecasting system WSFS that is currently operated in Finland, if certain criteria could be met. The SCA estimation process needs to produce an estimate for the error for each SCA value. In addition to that, the SCA data need to be processed without user intervention, preferably automatically, to make the implementation of the software for operational use as easy as possible.

The error estimation procedure was established using the law of error propagation. If the variations of the different variables in the estimation procedure are known, the error propagation can be used to produce a value describing the upper bound of the estimation error.

The formulation of an automatic processing system was a straight-forward software development problem. The various pieces of the software that had been written for the data analyses of ERS-2 and Radarsat-1 data were modified and combined to create an automatic processing chain. The system reads the satellite data in the format that is

produced by the satellite data provider, processes it, and produces SCA estimates and maps that can be utilized by the end-user. Development of software is typically a challenging and many-faceted process, and although it is a large and significant part of this Dissertation, it is not covered here. The final end-product, the automatic processing system, is briefly introduced to illustrate the system created.

3.3.1 Error Propagation analysis

The law of error propagation establishes the uncertainty of the estimation results by determining the uncertainty of each affecting variable in the estimation function (*Bevington and Robinson 1992*). This can be utilized to produce a statistical measure of accuracy for each SCA estimate. The accuracy information is important for operational use. For example, as SCA information is assimilated to a hydrological forecasting model the statistical accuracy of estimated is typically also required.

The law of error propagation provides the uncertainty of the SCA estimates based on the partial derivatives of the SCA estimation function

$$S_{SCA}^2 = \left(\frac{\partial SCA}{\partial \sigma^\circ_{surf}}\right)^2 S^2_{\sigma^\circ surf} + \left(\frac{\partial SCA}{\partial \sigma^\circ_{ground,\,ref}}\right)^2 S^2_{\sigma^\circ ground,ref} + \left(\frac{\partial SCA}{\partial \sigma^\circ_{snow,\,ref}}\right)^2 S^2_{\sigma^\circ snow,ref} \quad (3\text{-}3)$$

where S_{SCA}^2 is the variance of a SCA estimate, SCA is given by the equation (2-7), $S^2_{\sigma^\circ surf}$, $S^2_{\sigma^\circ ground,ref}$ and $S^2_{\sigma^\circ snow,ref}$ are the variances of the backscattering coefficients: the observed, the reference of snow free ground and the reference of snow-covered ground, respectively. When the partial derivatives are determined, the variance S_{SCA}^2 can be formulated as

$$\begin{aligned} S_{SCA}^2 = {} & \left(\frac{1}{\sigma^\circ_{snow,\,ref} - \sigma^\circ_{ground,\,ref}}\right)^2 S^2_{\sigma^\circ surf} + \left(\frac{\sigma^\circ_{surf} - \sigma^\circ_{snow,\,ref}}{\left(\sigma^\circ_{snow,\,ref} - \sigma^\circ_{ground,\,ref}\right)^2}\right)^2 S^2_{\sigma^\circ ground,ref} \\ & + \left(\frac{\sigma^\circ_{ground,\,ref} - \sigma^\circ_{surf}}{\left(\sigma^\circ_{snow,\,ref} - \sigma^\circ_{ground,\,ref}\right)^2}\right)^2 S^2_{\sigma^\circ snow,ref} \end{aligned} \quad (3\text{-}4)$$

This function gives the variance for each SCA estimate. In order to solve the variance of a SCA estimate, the variances for the reference backscattering coefficients need to be determined. The variances can be determined using available data, if they can be deemed to be adequately extensive. The Radarsat-1 SCW dataset used covers three snow-melt seasons, and each image consists of nearly two thousand analyzed drainage basins. It contains data from a relatively large geographical area, dominated by boreal forest. The variances were determined for the complete dataset and by dividing the data according to a few different categorization criteria, explained below.

During the snow-melt season, the backscattering coefficients depend mainly on the prevailing snow conditions. As snow status is the dominant factor, the variance of the reference backscattering coefficient needs to be determined for each SCA situation independently. This is done by dividing the backscattering coefficients according to the SCA conditions. For this study the backscattering coefficients were divided into ten separate SCA intervals: (SCA: 0%-10%, 10%-20%, 20%-30%,..., 90%-100%), and the variances for the backscattering coefficient $S^2_{\sigma^\circ surf}$ were calculated for each interval. Additionally, one category was used for the backscattering coefficients for the beginning of snow-melt season, relating to $S^2_{\sigma^\circ snow,ref}$ and one category for the end

of snow-melt season, relating to $S^2_{\sigma^\circ ground,ref}$. This categorization is taken as the baseline for this study. The baseline categorization results in very large categories with no consideration to, for example, the incidence angle of the observed drainage basin. Therefore, it is expected to produce slightly pessimistic uncertainty values. The variance of SCA can be expressed as a function of SCA when the observed backscattering coefficient σ^o_{surf} is formulated as a function of SCA

$$\sigma^\circ_{surf} = SCA\left(\sigma^\circ_{snow,\,ref} - \sigma^\circ_{ground,\,ref}\right) + \sigma^\circ_{ground,\,ref} \tag{3-5}$$

When this equation is combined with equation (3-4) the variance of SCA can be

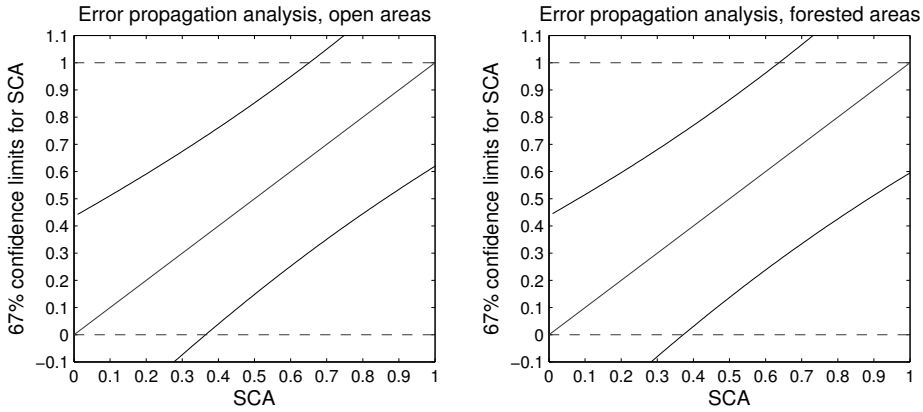

Figure 3-12. The error limits for SCA estimates derived by the error propagation analysis. The confidence limits were acquired with the baseline categorization; taking only the prevailing SCA conditions into consideration.

visualized. The baseline error limits are shown in Figure 3-12.

It is seen that the resulting errors are considerably larger than the SCA estimation accuracy acquired with the Radarsat-1 investigations would suggest. The average number of samples was 1448 in each category with the baseline categorization.

In order to produce more precise error estimates, the baseline dataset, which includes the categorization by prevailing SCA conditions, was further categorized according to incidence angle. The data were divided according to incidence angle using a step size of 1°. The variances were calculated for each category separately and the SCA error estimates are produced in a similar manner. The visualizations of the error limits, shown in Figure 3-13, are drawn using averaged variances, to produce one plot representing an average of all the categories.

It is seen from the Figure 3-13 that the error limits are closer to the expected magnitude and can be considered as more precise error estimates for the method. The average number of samples in each category was 54 in this approach.

The error propagation analysis seems to provide plausible results when an appropriate categorization is implemented. Incidence categorization seems to provide reasonable uncertainty values.

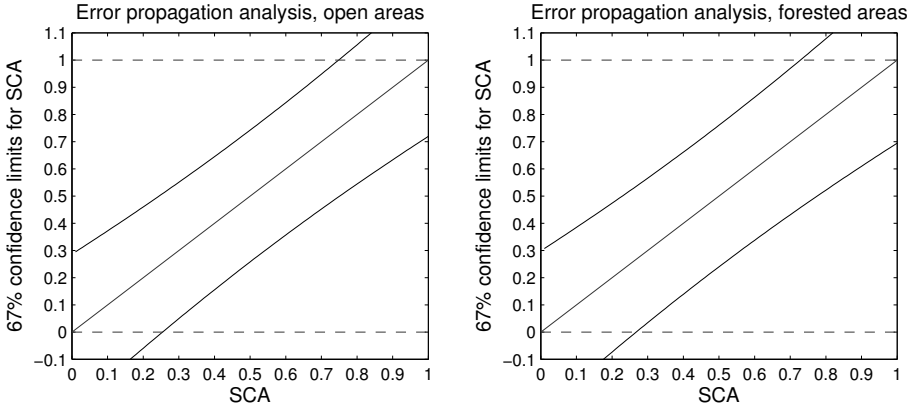

Figure 3-13. The error limits for SCA estimation derived by the error propagation analysis. The confidence limits were acquired with the incidence angle categorization.

3.3.1.1 The error propagation analysis compared with the Radarsat-1 SCW-based accuracy characterization

One important issue was to determine the interconnection of the error propagation analysis to the accuracy analyses conducted with the MODIS-based comparison data, presented in [P2]. A conventional scatter plot presenting the agreement of reference and estimated data was drawn along with a visualization of the average SCA estimates and the standard deviation of the SCA estimates. These two visualizations were combined with the error propagation analysis Figure 3-13.

The combined figures reveal the overall agreement for the error propagation analysis and the true behavior of the SCA method when compared to reference data. The results are shown in Figure 3-14. The agreement between the error propagation analyses and the actual reference data validation is clearly observed. The scatter plot seems rather well behaved, even as there are more than 9020 samples drawn on the figure. The plot showing the average SCA estimates and the standard deviations of the samples have good agreement with the error propagation analyses.

Categorization by incidence angle seems to show a slight overestimation for the uncertainty. It can be concluded that the error propagation analyses agree well with the actually observed data, i.e., the SCA estimates compared to the reference data.

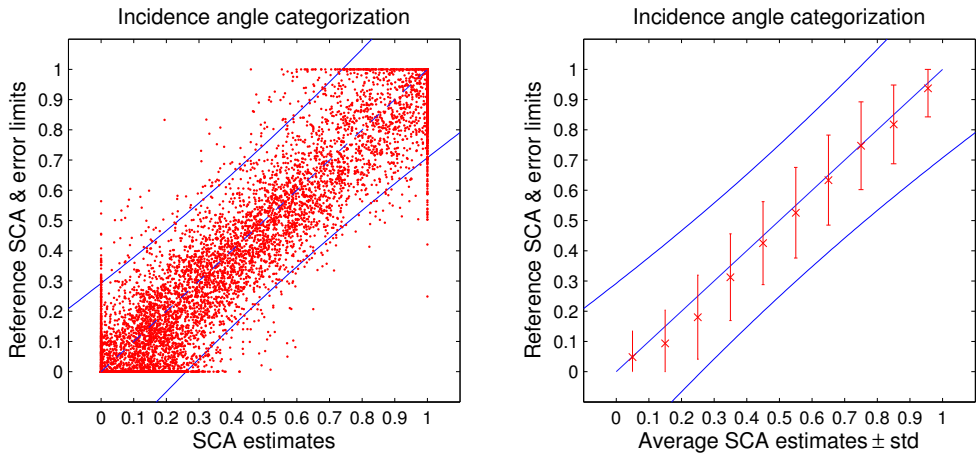

Figure 3-14. The error limits for SCA estimates derived by the error propagation analysis plotted with the SCA estimate and reference SCA comparison. The confidence limits were acquired with the incidence angle categorization. The left hand plot shows the scatter plot between the Radarsat-1 SCW-based estimates and the optical reference data. The right hand plot shows the average SCA estimates and the standard deviation of the samples, derived from the SCW-based SCA data.

3.3.2 Realization of an automatic processing system for SCA estimation

The functioning of the developed automatic processing software for SCA estimation is presented in detail in [P6]. The software reads raw satellite images as input and produces finalized SCA estimates and maps. The software can utilize C-band spaceborne SAR intensity images. The nominal adaptation has been done for Radarsat-1 SCW-data. The SCA maps are generated from the actual satellite images based on the enhanced TKK SCA estimation method described in the previous Sections. The SCA estimation software is implemented using Matlab and has a modular structure. Each module performs a part of the overall SCA estimation task.

A brief overview of the processing system:

- The satellite image (in CEOS format) is rectified and calibrated using a TKK developed custom program (*Kärnä et al. 2005*).
- The image is rectified and aligned to a common reference coordinate system with the reference data.
- The backscattering coefficients and incidence angles are calculated for each computational unit (drainage basin) and each forest stem volume category.
- A forest compensation algorithm is used to determine a computational backscattering coefficient for forested areas.
- The backscattering values are used to determine the SCA estimates independently for open areas and forested areas.
- An error estimate is calculated for each SCA value based on the error propagation analyses
- The weather station assimilation method is used to evaluate and correct possibly false SCA estimates
- The snow-covered area estimates are visualized in a SCA map

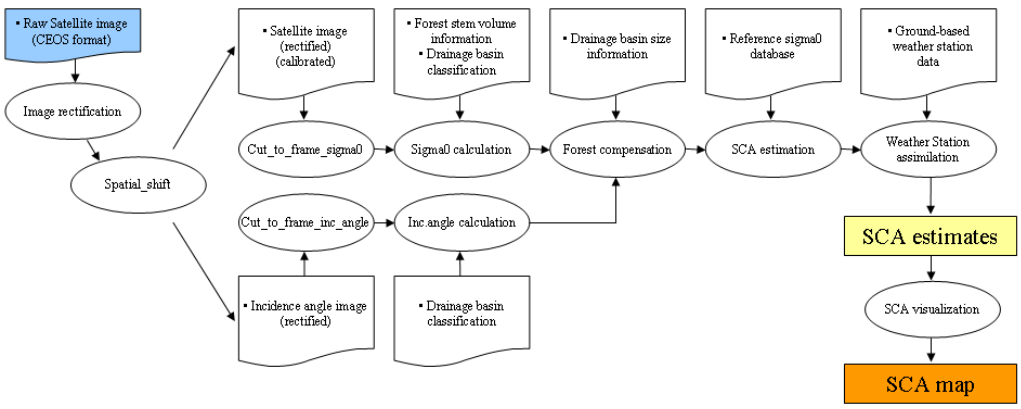

Figure 3-15. A flowchart presenting the automatic SCA estimation software.

A flowchart illustrating the processing chain is shown in Figure 3-15.

The starting point for the processing is satellite data provider-produced satellite images in CEOS (Committee on Earth Observation Satellites format. There are two outputs from the processing chain: the SCA maps and the SCA estimates. A total of three maps are created: a map for open areas, a map for forested areas and a combined map for open and forested areas. The SCA maps are image files in TIFF format. The SCA estimates are stored in a matrix with an estimate for open, forested and the combined case. An error estimate based on the error propagation analyses presented in the previous Section is calculated for each SCA estimate and stored within the result file. An example of an SCA map drawn by the software is seen in Figure 3-6.

The implemented processing chain utilizes various types of reference data, such as the forest stem volume classification of the target area, the drainage basin classification, information of the reference backscattering values for each drainage basin, the weather station data and a visual presentation of the Finnish national borders. The backscattering reference data are a by-product of the snow research conducted at TKK. The other reference data are provided by SYKE for research purposes and utilized in SYKEs own operational monitoring activities and are not available as public domain.

3.3.2.1 Limitations of the TKK SCA method and the processing system

The processing system works with data that have been acquired and are stored in the system. It is not able to fetch or transfer data from an outside database. Typically the satellite data need to be ordered in advance from the satellite data provider and they need to be fetched by, for example, an ftp program. These are steps that need to be conducted by the user. Otherwise the processing system can be set up to process data completely automatically without user intervention.

The snow-covered area estimation method has been designed to measure the SCA during the snow-melt season. The method does not function during the winter season when the snow pack is typically dry. The estimation does function after the end of snow-melt season, if weather station data are available. In the absence of the weather

station data, the method does not produce accurate SCA estimates under the conditions of the post snow-melt season.

The theory behind the SCA estimation assumes that the observed snow pack is wet, as is normally the case during the snow-melt season. However, if the method is implemented when the snow pack is dry (i.e. during the very early snow-melt season when the temperature is still dominantly well below zero degrees Celsius) the backscattering coefficients can be significantly higher. In this case the method results in SCA values significantly less than 100% even though the ground is still covered by snow. To overcome these limitations, it is recommended to monitor the prevailing weather and snow conditions when interpreting the results of the SCA estimation.

More detailed information of the processing system and a brief user manual are presented in [P6].

3.3.2.2 Monitoring of SCA on a continental or global scale

Utilization of the forest compensation and the weather station assimilation procedures require access to the relevant supplementary data. If these are not available, the methodology does not achieve its optimal performance. As far as the land areas of Finland are concerned, this is not an issue, but adapting the method for global monitoring would be significantly more challenging.

The simpler method described in Section 2.4, proposed originally by (*Rott and Nagler 1993*) and utilizing a single reference image for SCA estimation is a more convenient method when considering SCA monitoring on a global scale. The performance of the single reference image method on the boreal forest zone is investigated and compared with the TKK method in the following Section.

3.4 Comparison of the proposed SCA estimation methods

Two distinct approaches have been proposed for SCA monitoring by spaceborne SAR. The method utilizing a single reference image, originally proposed by (*Rott and Nagler 1993*), was explained in Section 2.4. The other approach is the TKK SCA estimation method, discussed throughout this dissertation.

The single reference image approach has been widely adopted and it has been shown to perform well on mountainous and other non-forested areas (*Baghdadi et al. 1997, 2000, Nagler and Rott 2000, Malnes and Guneriussen 2002*). As the single reference image method is easier to implement, it is more suitable for monitoring of very large areas, such as continental or global scale. It was therefore of great interest to determine its accuracy on the boreal forest zone. The accuracy of the method for mountainous areas reported by (*Nagler and Rott 2000*) shows an agreement of approximately 83% when snow maps derived from Landsat-5 Thematic Mapper (TM) data are compared with SAR-based maps; the investigation considers the classification of the pixels for either snow-covered or snow-free classes. The agreement of 83% means the percentage of correctly classified samples. The accuracy of the method investigated for mountainous regions of Scandinavia by (*Malnes and Guneriussen 2002*) shows an error rate of 17%. The investigation, derived according to Bayesian statistics, evaluates the classification between wet snow and dry snow pixels. The error rate of 17% gives the fraction of falsely classified samples.

The accuracy for the single reference image method on boreal forest zone was evaluated using the same Radarsat-1 dataset as used for the TKK method in Sections 3.2 and 3.3, thus making it easy to compare the two methods with each other. The complete investigation is presented in [P4].

Several aspects regarding the SCA estimation methodologies were analysed: a) the suitable threshold level for the single reference image method on the boreal forest zone, b) the estimation accuracy difference when a single or two reference images are used and c) a comparison between the single reference image and the enhanced TKK SCA estimation methods.

3.4.1 Evaluation of the single reference image method

The single reference image SCA method distinguishes wet snow-covered areas from bare ground, based on the backscattering difference between the two. The authors (*Nagler and Rott 2000*) suggest using a three decibel threshold to separate the snow-covered areas from the snow-free ground. A more modest threshold level is suggested by (*Magagi and Bernier 2003*). Additionally, the backscattering levels observed on the boreal forest zone (see [P4]) suggest that a smaller threshold level may yield more accurate SCA estimates. Also, the selection of the reference image will probably affect the optimal level of the estimation threshold.

The analyses were carried out separately for each reference image investigated. The accuracies acquired using the suggested -3dB threshold showed very poor agreement with the optical comparison data (RMSEs between 0.308 and 0.446; and 0.381 in average).

The optimal threshold level for each reference image was determined using the optical comparison data. The threshold level that produced the best agreement between the SAR-based estimation and optical comparison data was selected for further analysis.

For dry-snow reference images the optimal threshold levels in the boreal forest zone were 0.0 dB, -0.4dB, -0.35dB and 0.0 dB. The RMSE values obtained were between 0.176 and 0.203 (with an average of 0.186) and the correlation coefficients were between 0.908 and 0.836. The optimal reference image was from 27 March 2007 and the optimal threshold level for it was -0.4 dB. The effect of the threshold level on SCA estimation accuracy is shown in Figure 3-16. It is seen that the estimation accuracy varies dramatically with different threshold levels. A threshold level of 0.0 dB (which was optimal for two of the dry snow images) means that backscattering coefficients that are lower than the reference are determined to be wet snow and backscattering coefficients that are higher are classified as bare ground.

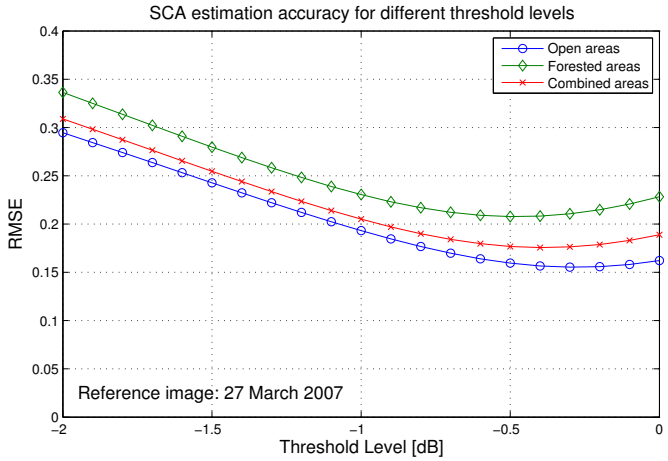

Figure 3-16. The effect of threshold level on SCA estimation accuracy shown for the single reference image method. The accuracy is shown for the optimal reference image of 27 March 2007 (dry snow), which yielded the best SCA estimation accuracy. Radarsat-1 SCW data were used for the analyses.

The results with bare ground reference images were slightly different. Threshold levels of -1.4 dB, -1.2 dB, -1.3 dB and -0.5 dB produced the best SCA estimation results. The obtained RMSE values were between 0.193 and 0.210 (with an average of 0.200) and the correlation coefficients were between 0.880 and 0.854. The optimal bare ground image was from 12 May 2006 and had an optimal threshold level of -0.5dB. The images were acquired with a different amount of time after the end of the snow-melt season, and thus had a significant variation in their ground wetness and their respective backscattering levels. The optimal threshold level is directly proportional to the ground wetness and, hence, the temporal difference from the snow-melt season.

The SCA estimation accuracy obtained with the optimal reference image of 27 March 2007 and optimal threshold is shown in Figure 3-17a. These analyses show that it is very important to find the optimal threshold level when adapting the single reference image method to a new geographical location.

3.4.2 Comparison of the TKK and the single reference image SCA methods

The TKK SCA estimation method is composed of several elements. The main difference with the single reference image method is the utilization of two reference images. There are, however, additional enhancements to the method that are also examined. The comparison is carried out in regard to the enhanced TKK method that consists of the following elements 1) the linear interpolation using two reference images 2); the forest compensation procedure; and 3) the weather station assimilation procedure and reference image selection process on a computational unit scale.

The best attainable SCA estimation accuracy using a single reference image had an RMSE of 0.176. Evaluation of the same dataset, with two reference images, from 18 April 2004 and 26 May 2004, showed an RMSE of 0.156 for SCA estimation. The accuracy is further illustrated in Figure 3-17b. Comparing the Figures 3-17a and 3-17b it is evident that the method using two reference images produces significantly less biased estimates near the beginning and the end of snow-melt seasons. Finding the optimal threshold level for the single reference image method determines the cut-

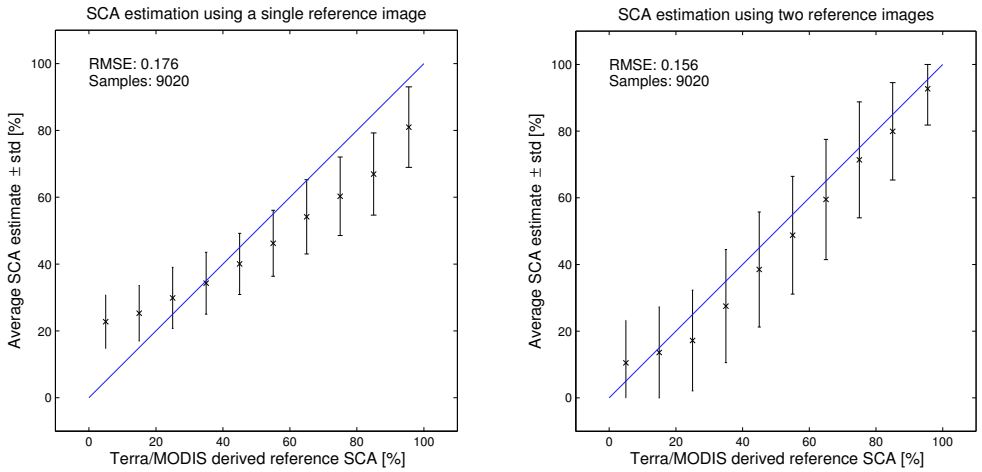

Figure 3-17. SCA estimation accuracies shown for the different methods. The left-hand side image shows the best obtained accuracy for the single reference image method. The right-hand side image shows the accuracy using two reference images and no forest compensation. Radarsat-1 SCW data were used for the analyses.

off backscattering level for wet snow/bare ground discrimination but this does not seem to be sufficient to produce an accurate SCA estimate throughout the whole melting season on boreal forests.

The SCA estimation accuracy with two reference images and the forest compensation procedure yields an RMSE of 0.151. The SCA estimation accuracy for the enhanced TKK method with all the elements enabled attains an RMSE of 0.123, and is shown in Figure 3-11.

It can be concluded that the difference in SCA estimation accuracy when using a single or two reference images is notable. The difference in estimation accuracy is even greater when the single reference image method is compared with the enhanced TKK SCA estimation method.

3.4.3 The effect of forest fraction on SCA estimation accuracy

Prior investigations in [P2] and [P3] indicate that the SCA estimation accuracy is affected by the amount of forestation on the evaluated areas. Therefore, the estimation accuracy was investigated for the cases where the evaluated drainage basins consist mostly of open or forested areas. The evaluations were carried separately for the areas that had more than 75% and the areas with less than 25% forested pixels. The accuracies were evaluated for both the single reference image method with optimal reference image and threshold and for the enhanced TKK estimation method. The accuracy of the single reference image method on areas with more than 75% of forests shows an RMSE of 0.226, and the accuracy for the TKK method yields an RMSE of 0.154 for the same areas. There were a total of 516 samples for the forested areas. The accuracies for the areas with less than 25% of forest shows an RMSE of 0.151 for the single reference image method, and the accuracy for the TKK method yields an RMSE of 0.117. There were a total of 1844 samples for the open areas.

It is evident that for heavily forested areas the difference in estimation accuracy is larger between the two different methods. Additionally, the TKK method produces more accurate estimates also for open (non-mountainous) areas.

3.4.4 Conclusions for the single reference image SCA estimation method

The optimal threshold level for SCA estimation using a single reference image was between -0.0dB and -1.5dB, largely depending on the selected reference image. The lower optimal threshold, than that observed for the mountainous regions, is mainly due to the different backscattering characteristics of the boreal forest zone; i.e. the backscattering contribution of forests decrease the contribution of surface snow conditions on the overall observed backscattering signature. The optimal threshold level for the dry snow image that produced the best estimation accuracy was -0.4 dB; this yielded an RMSE of 0.176. The average RMSE for SCA estimation using a single reference image, when the optimal threshold level had been determined for each reference image, was 0.193. The accuracy is significantly weaker than that of the TKK method developed specifically for boreal forest regions. Accuracy of the TKK method, using the exact same dataset showed an RMSE of 0.123. The TKK method, as the single reference image method, can be operationally used with historical reference data from previous years, as shown in [P2].

The investigation shows that the single reference image method is usable for the boreal forest zone, although the accuracy is limited and poorer than that of the method using two reference images; however the clear benefit of the single reference image method is its easier implementation for observation of very large areas, i.e. on a continental or global scale.

3.5 Effects of snow wetness on snow-melt monitoring

As space-borne C-band SAR observations are used for monitoring the snow cover during the spring melt period, temporal changes in backscattering properties of forest cover affect the estimation of snow cover properties as shown in the previous Sections. In addition to the influence of forest cover, snow wetness has a significant effect on the observed backscattering coefficient during the snow-melt season. The inversion of a combined forest/snow/ground backscattering model to yield estimates for the relative changes of snow wetness during full snow cover conditions is validated in [P5].

The performance of the snow wetness estimation algorithm, as well as the validity of the backscattering model employed, was tested for the Kemijoki river drainage area in Northern Finland. Time series of ERS-2 C-band SAR images and ground truth data for eight test regions representing the winter/spring periods of years 1997 to 2002 were used for analyses.

The investigations were performed for eight separate test areas, each of which covered a region of 15 km x 15 km around a weather station. The available reference data included the weather station observed temperature information, snow depth information, precipitation information and SCA information (all measured in the vicinity of weather stations). The analyses were carried out for each region using mean backscattering coefficients for non-forested areas and forest compensated values for the forests.

3.5.1 The snow wetness model

The snow backscattering contribution, σ°_{snow} in SCA estimation (see equation (2-6)), can be modeled as a function of the volumetric liquid water contribution of the snowpack (or top snow layer). If all the other factors affecting the level of observed σ° are known, it is possible to retrieve estimates of liquid water content by inverse solution of snow and ground backscattering models (Section 2.3). In practice, all the relevant factors are typically not known, which deteriorates the estimation accuracy, especially if only single-channel SAR observations are available. However, it is possible to obtain information on the relative temporal changes of moisture levels even from single-channel SAR data on a regional scale if other relevant parameters can be treated with effective spatially/temporally averaged values (these average values can be based, for example, on reference *in situ* data).

In the investigation [P5], the estimation of liquid water content of snow and ground (soil) is restricted to cases representing 100% snow cover conditions. The snow backscattering model is a discrete scattering approach-based semi-empirical model described in (*Koskinen 2001*). It considers the total observed backscattering as a combination of 1) backscattering from the snow-air interface, 2) volume scattering from the snow layer and 3) backscattering from the underlying ground surface, including the two-way transmissivity of the snow layer:

$$\sigma^{0}{}_{snow} = \sigma^{0}{}_{snow\text{–}air} + \sigma^{0}{}_{snow\text{–}vol} + \sigma^{0}{}_{snow\text{–}ground} \tag{3-6}$$

The snow-air surface backscattering contribution $\sigma^{\circ}_{snow\text{-}air}$, essential under wet-snow conditions, is treated with the IEM model (*Fung 1994*):

$$\sigma^{0}_{snow\text{–}air} = 4\pi \cos\theta_s \left[I_p(\mu_s, \phi_s) / I^i{}_p \right] \Big|_{\theta_s = \theta} = \frac{k^2}{2} \exp\left(-2k_z{}^2 s_s^2\right) \sum_{n=1}^{\infty} \left| I^n{}_{pp} \right|^2 \frac{W^n(-2k_x, 0)}{n!} \tag{3-7}$$

where θ_s is the reflection angle, θ is the incidence angle, I_p is the incident or scattered power intensity, μ_s is the cos of the scattering angle, ϕ_s is the azimuth angle, k is the wave number, k_x is [k cos θ], k_z is [k sin θ], s_s is snow surface RMS-height, I_{pp} is scattering intensity term and W is the surface correlation function for which the exponential function was applied. The snow volume scattering contribution $\sigma^{\circ}_{snow\text{-}vol}$ is approximated using a volume scattering model developed for layers with small dielectric constant (*Fung 1994*):

$$\sigma^{0}{}_{snow\text{–}vol} = 0.5\omega \cdot T_{lt} T_{tl} \cos\theta \left[1 - \exp\left(-\frac{2\tau}{\cos\theta_t} \right) \right] P_{pp}(\cos\theta_t, -\cos\theta_t; \pi) \tag{3-8}$$

where ω is the snow volume scattering albedo, T_{lt} is the Fresnel power transmission coefficient τ is optical depth , P_{pp} is the phase function of volume scattering and θ_t is the transmission angle.

The soil backscattering contribution $\sigma^{\circ}_{snow\text{-}ground}$ is described by the empirical model from (*Oh et al. 1992*). Altogether, the snow backscattering model is simple enough to be applied in iterative inversion by using a minimization procedure similar to equation (3-2). In the case of snow liquid water content estimation from ERS-2 SAR data we can write the estimation algorithm as:

$$\min_{m_{v,snow}} \left| \overline{\sigma}^{\circ}_{surf} - \sigma^{\circ}_{snow}(m_{v,snow}, \langle s_s \rangle, \langle l \rangle, \langle d_0 \rangle, \langle \rho \rangle, \langle h \rangle, \langle s_g \rangle, \langle \varepsilon_g \rangle) \right| \qquad (3\text{-}9)$$

where the parameters of snow model include, in addition to snow wetness $m_{v,snow}$, snow surface RMS-height s_s, horizontal snow surface correlation length l, effective snow grain size d_0, snow density ρ, snowpack thickness h, ground surface RMS-height s_g and soil dielectric constant ε_g. The estimate for ground surface backscattering contribution σ°_{surf}, (scalar variable) is obtained by (2-6) as the whole ground is assumed to be covered by snow (SCA = 1 in equation (3-2)).

All parameters in (3-6), except $m_{v,snow}$, have to be dealt with *a priori* mean values in the estimation of snow wetness. Fortunately, most of these parameters have only marginal effect on σ°_{snow}, e.g. ground surface parameters and snowpack thickness in the case of wet/moist snow cover. The most serious problem with the estimation of snow wetness according to procedure (3-6) is caused by temporal variations of snow grain size d_0 and snow surface roughness properties (s_s and l).

3.5.2 The estimation of effective snow wetness

The surface or forest floor backscattering contribution σ°_{surf} determined by (3-1) and (3-2) can be used for estimating the effective snow wetness under conditions with 100% snow cover. Figure 3-18 shows the correlation between backscattering coefficients calculated for open areas and 3-day average temperature values. The 3-day minimum, mean and maximum temperatures were calculated averaging daily minimum, mean and maximum values from three days. Figure 3-18 shows strong correlation (R^2 = 0,72-0,63) between various 3-day average temperature values and the backscattering coefficient. These high correlation values suggest that the strongest influence on the backscattering coefficient is due to snow wetness.

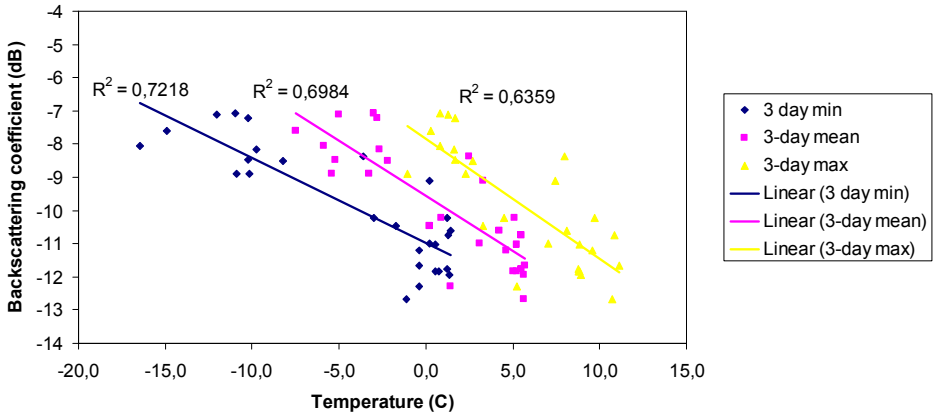

Figure 3-18. Comparison of backscattering coefficients derived for open areas around the weather stations with 3-day average values of daily minimum, average and maximum temperatures. The linear correlation curves and R² values are shown for each case. ERS-2 data were used for the analyses.

Figure 3-19 shows the snow wetness estimation results obtained by applying (3-9) for all snow observations with 100% snow cover from 1997 to 2002. This analysis includes also forested areas where the contribution of forest canopy is removed using equations (3-1) – (3-2). The moisture estimates are compared with 3-day mean

temperatures. The curve plotted in Figure 3-19 presents the fitting of a logarithmic function to the estimates. The results indicate that even a single channel C-band SAR can be used for detecting temporal changes in snow wetness. Also, estimates from forested areas show reasonable values and agree well with those from open areas. Obviously, the absolute scale is not accurate as snow grain size and snow surface roughness properties are considered invariant with time.

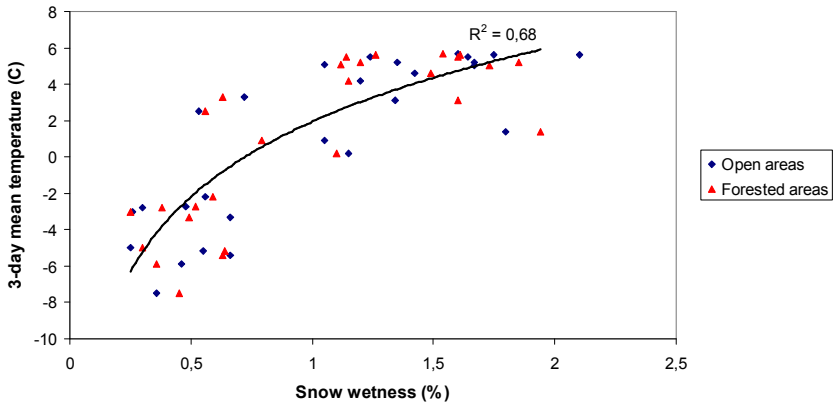

Figure 3-19. Snow wetness estimates obtained for conditions with 100% snow cover. The results are depicted as a function of weather station-observed 3-day average daily temperature. The pre-fixed model parameter values used are: ⟨s⟩ = 6 mm, ⟨l⟩ = 5 cm, ⟨d_0⟩ = 2.8 mm (effective snow grain size that is larger than the physical grain size), ⟨ρ⟩ = 0.3 g/cm^3, ⟨h⟩ = 1 m, ⟨s_g⟩ = 1.2 cm and ⟨ε_g⟩ = 6 – 1j (frozen soil with some liquid water inclusions). ERS-2 data were used for the analyses.

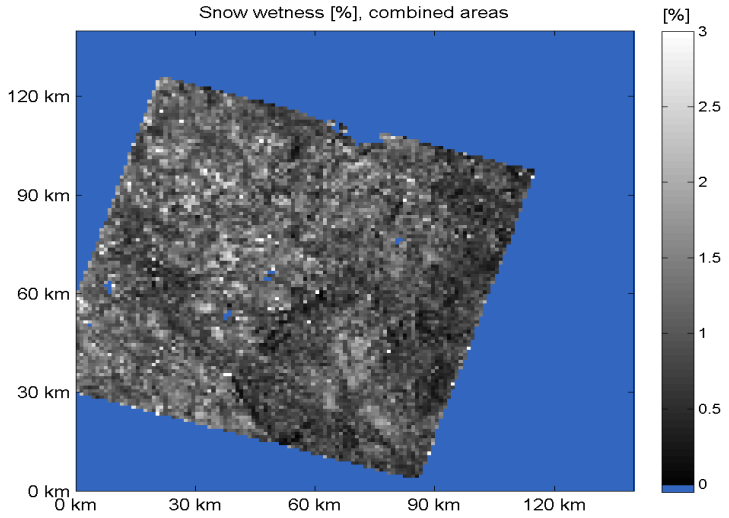

Figure 3-20. Snow wetness estimated from a single ERS-2 SAR image taken 23 April 2001. The pre-fixed model parameter values used are: ⟨s⟩ = 6 mm, ⟨l⟩ = 5 cm, ⟨d_0⟩ = 2.8 mm (effective snow grain size that is larger than the physical grain size), ⟨ρ⟩ = 0.3 g/cm^3, ⟨h⟩ = 1 m, ⟨s_g⟩ = 1.2 cm and ⟨ε_g⟩ = 6 – 1j (frozen soil with some liquid water inclusions).

Figure 3-20 shows a sample snow wetness map calculated from a single SAR scene. The image was taken on 20 April 2001. The forest contribution is removed using the forest model according to (3-1) – (3-2) and the snow wetness is calculated using the snow backscattering model (3-6) – (3-9) and parameters introduced in this Section. The calculation is carried out for a 1 km x 1 km grid. The image displays the variation of effective snow wetness: as is to be expected, the snow wetness estimates logically decrease towards the eastern end of the image where the temperatures are colder and snow is also dryer according to weather station observations. In the east the snow wetness flag turned to wet snow only 2 days earlier while in western areas the flag has been on wet snow for 5 to 8 days.

3.5.3 Conclusions for the snow wetness estimation

The highest effect on the total backscattering from snow cover in a non-mountainous boreal forest region is due to snow wetness. When the area is totally covered by snow the effective changes of snow wetness can be monitored by employing a simple backscattering model that will describe the backscattering from the snow-air interface, the snow volume and the snow-soil interface. If high spatial resolution reference data on boreal forest stem volume or biomass is available, the inverse solution of the semi-empirical forest backscattering model yields realistic information about the relative temporal changes in snow wetness in forested areas during conditions with a full snow cover.

4 CONCLUSIONS

Previous investigations of snow monitoring using spaceborne SAR on the boreal forest zone have been carried out by (*Koskinen et al. 1994*, *Koskinen et al. 1997, Pulliainen et al. 2001*). Corresponding investigations for mountainous regions have been carried out by (*Rott and Nagler 1993, Guneriussen et al. 1996, Shi and Dozier 1997, Nagler and Rott 2000*). The work described within this dissertation is focused on the boreal forest zone and is a continuation of the work described in (*Koskinen et al. 1997, Pulliainen et al. 2001*).

The aim of this dissertation was the further development of SAR-based snow monitoring methodologies. The central element was the refinement of the TKK SCA estimation method, which utilizes satellite-based C-band SAR for SCA estimation on the boreal forest zone and is intended for operational snow monitoring applications during the spring melt-season. The main contribution of this dissertation for the field of remote sensing is the building of SAR-based snow monitoring capabilities for the boreal forest zone.

The main objectives for the dissertation were (as listed in Section 1.2):

(1) to develop an operationally feasible SAR-based SCA estimation methodology for boreal forest region [P1], [P2], [P3],

(2) to characterize the accuracy of SCA estimation for the boreal forest zone using the developed methodology [P1], [P2], [P3],

(3) to develop a feasible method for producing uncertainty information for the SCA estimates and to investigate the automation of the SCA estimation method, including the development of an demonstration system that can be utilized in operational hydrological monitoring [P2], [P6] and

(4) to evaluate the feasibility of the existing SAR-based SCA estimation methods for the boreal forest zone [P4] and to improve the understanding of the behavior of snow backscattering signatures during the snow-melt season [P5].

The main accomplishments of this dissertation, published in [P1]-[P6], include:

(1) validation of the forest compensation methodology for SCA estimation,

(2) accuracy characterization of the TKK SCA estimation method (using both ERS-2 and Radarsat-1 SAR data),

(3) validation of wide-swath SAR utilization for SCA estimation on the boreal forest zone,

(4) an error propagation analysis for the TKK SCA method, enabling the implementation of the method for operational near-real time hydrological applications,

(5) demonstration of the feasibility of multi-year reference data for SCA estimation using the TKK method,

(6) incorporation of a weather station assimilation methodology for SCA estimation,

(7) development of a reference image selection procedure on a computational unit level,

(8) development of an automatic processing system for SCA estimation employing the TKK method,

(9) comparison of the existing SCA estimation approaches for boreal forests

(10) investigation of C-band SAR capabilities for evaluation of snow wetness utilizing a semi-empirical modeling approach

The listed accomplishments support the set objectives (1)-(4) and one of the outcomes of this work is an operationally feasible SCA estimation methodology that has been implemented into operational use by the Finnish Environment Institute. In addition, the knowledge concerning SAR-based snow monitoring methodologies on the boreal forest zone has significantly increased.

The significance of the main accomplishments includes:

- The validation of the forest compensation methodology was carried out using SAR data of ERS-2 and Radarsat-1. The investigations showed that the SCA estimation accuracy was significantly increased by the utilization of the forest compensation algorithm. Additionally, in densely forested areas, its influence was even more highlighted.
- The statistical accuracy characterizations [P1]-[P3] showed an RMSE of 0.193 (average for open and forested areas) using ERS-2 data and the standard TKK method. The characterization using the Radarsat-1 data for the standard TKK method showed an RMSE of 0.151. The estimation accuracy for the enhanced TKK method showed an RMSE of 0.123 using the Radarsat-1 dataset. The accuracy characterizations also clearly showed that the estimation accuracy is independent of the incidence angle.
- An error propagation analysis was conducted for the TKK method [P2]. The analysis was validated by comparing the results of the analysis with the conducted accuracy characterizations. The results of the error propagation analyses enable the utilization of the TKK method for operational use [P6]. The TKK SCA method has been taken into operational use by the Finnish Environment Institute.
- Demonstration of the multi-year reference data utilization enables the use of the TKK method in an operational manner by employing historical data as reference [P2]. Using the reference data from previous years, the SCA estimation can be carried out during the snow-melt season [P2], which is a vital prerequisite for operational applications.
- The weather station assimilation procedure prevents the formation of possibly erroneous SCA estimates after the end of the snow-melt season has been reached. The accuracy characterizations showed in increase in estimation accuracy from an RSME of 0.151 to an RMSE of 0.140 even with a limited set of comparison data (that lacked the most obviously improved cases) [P3].

- The reference image selection procedure on a computational unit scale makes the method easier to adapt to new environments and showed an increase in SCA estimation accuracy: the RMSE improved from 0.151 to 0.136 [P3].
- The developed automatic processing system enables the employment of the TKK SCA method for hydrological simulation and forecasting applications [P6].
- The comparison of the SAR-based SCA estimation methods determines the performance and feasibility of the different approaches on the boreal forest zone. The analyses can be used by potential end-users when selecting the methodologies for implementation on boreal forest region [P4]. The accuracy for the single reference image method showed an average RMSE of 0.193 and the best achieved performance, an RMSE of 0.176, when applied on the boreal forest dominated test region.
- The feasibility of the C-band SAR and the combined forest/snow/ground backscattering model to yield estimates for the relative changes of snow wetness during full snow cover conditions was investigated [P5]. The correlation between the backscattering coefficients and the model-derived snow wetness data are significant. The modeling approach can be used to determine the changes in snow wetness during full snow-cover conditions.

For regional scale applications the developed methodology has been found to be well usable. For operational applications the method can be employed using historical reference image data, thus near-real time monitoring is feasible. To date the methodology has been successfully employed in operational use for several snow-melt seasons, in practice by assimilating the SCA-values determined from Radarsat-1 observations to the watershed simulation and forecasting system (WSFS) of SYKE. The methodology can also be used for areas without forest stem volume data, simply by skipping the forest compensation phase. The lack of forest data decreases the estimation accuracy proportionally to the forest density and could be accounted for by using more pessimistic uncertainty values.

The investigations carried out within this dissertation are regionally and geographically limited and the achieved estimation accuracy is likely to vary in different regions. The main advantages of the method are seen on the boreal forest regions; for mountainous regions the method developed by (*Nagler and Rott 2000*) is probably more appropriate due to its well established characteristics (on mountainous regions) and its easier implementation (requirement for a single reference image and no need for forest stem volume or weather station data). The feasibility of the TKK method, however, for areas like boreal forest regions of Siberia, northern Russia and Canada are probably quite suitable and this would be a worthy direction for future investigations.

For climate monitoring applications the availability of data on a regional scale are not sufficient. Instead, continental or global scale data are needed and preferably for as long a time series as possible. In order to produce snow information on a continental or global scale the TKK methodology would need to be evaluated and characterized for the different regions. Additionally, the monitoring of large areas using the currently available SAR data is challenging due to the limitations of the spatial coverage achieved. Monitoring continental scale regions on a weekly or even a

monthly basis is not feasible using the current satellite data (Envisat ASAR, Radarsat-1/-2), since the data are available by request only, the instruments do not acquire data continuously from all the regions and the data are costly. However, in the future there are a few promising SAR satellite missions that could provide means to monitor snow conditions on a global scale. The foremost satellite, GMES/Sentinel-1, with an existing budget and a launch date (currently) around 2011-2012, is carrying a C-band SAR instrument comparable to the Radarsat-1 SAR. The data provided by the Sentinel-1 are currently envisioned to be distributed free of charge and the expected spatial coverage will be more extensive than that of the current generation instruments. These C-band data and the TKK SCA methodology could be used to monitor the snow cover properties on a continental or global scale on selected regions. This would require the characterization of the TKK method for the different regions.

5 SUMMARY OF APPENDED PAPERS

[P1]

In Publication [P1], the TKK-developed SCA estimation method for boreal forest zone is investigated using a large dataset of multi-year observations. The publication establishes the statistical accuracy of the method compared with reference data obtained from hydrological modeling. The snow-covered area estimation method is evaluated using spatially limited SAR imagery from ERS-2. In addition to the assessment of statistical accuracy, the effect of forest compensation is analyzed, the utilization of multi-year reference imagery is validated and the effects of imaging geometry, topography and snow conditions are evaluated for SCA estimation.

[P2]

Publication [P2] evaluates the employment of wide-swath SAR data for operational SCA estimation using the TKK method on the boreal forest zone. The issue is investigated by comparing Radarsat-1 ScanSAR Wide A-based SCA estimates with spaceborne optical remote sensing data. The investigation shows that the SCA estimation is feasible using wide-swath data with large variations in incidence angle within the different image elements. The method is shown to perform well, achieving a correlation coefficient of 0.923 and RMSE of 0.145 when SAR-based SCA estimates are compared with the reference data on snow-melt seasons of 2004 and 2005. An error propagation analysis presented in the publication enables the operational implementation of the TKK SCA estimation method in hydrological simulation and forecasting.

[P3]

An enhanced SCA estimation method for the boreal forest zone is presented in publication [P3]. The enhanced method utilizes a fusion of Radarsat-1 and ground-based weather station data for SCA estimation and demonstrates a new process for reference image selection on a computational unit scale. The accuracy of the enhanced method is determined using spaceborne optical remote sensing data as reference for the snow-melt seasons of 2004-2006 in northern Finland. The method is shown to improve the estimation accuracy and achieves a correlation coefficient of 0.949 and an RMSE of 0.123 when the SAR-based SCA data are compared with Terra/MODIS-based SCA estimates. Additionally, the TKK method is adapted to produce SCA estimates with a spatial resolution of 5 km x 5 km. The analyses for the 5 km x 5 km method indicate poorer estimation accuracy than the nominal drainage-basin-based method.

[P4]

Publication [P4] characterizes the estimation accuracies of two SAR-based SCA estimation methods on a boreal forest-dominated test area in northern Finland. The methods evaluated are the enhanced TKK method and a method developed for mountainous regions, utilizing a single reference image for SCA estimation. The analyses are carried out using Radarsat-1 data for the snow-melt seasons of 2004-

2007. The SCA estimation accuracies for the SAR-based methods are determined using optical satellite based SCA data as reference. The results show that SCA estimation using a single reference image is usable for boreal forest zone, although the accuracy is significantly weaker than that of the TKK-developed, boreal forest-specific SCA method. The best accuracy obtained shows an RMSE of 0.176 for the single reference image method and an RMSE of 0.123 for the TKK SCA method. Additionally, the optimal threshold level for SCA estimation on the boreal forest zone using the single reference image method is investigated.

[P5]

Publication [P5] presents an analysis of snow properties in the vicinity of eight weather stations for both open and forested areas in northern Finland. The investigation validates the inversion of a combined forest/snow/ground backscattering model to yield estimates for the relative changes of snow wetness during full snow cover conditions. A comparison of the baseline TKK SCA estimation method in regard to weather station observations is also carried out. The results show that under all investigated conditions the semi-empirical forest backscattering model describes the average C-band backscattering properties of all test regions as a function of forest stem volume with a high performance. The retrieved relative snow wetness values show good agreement with *in situ* observations.

[P6]

Automatic software for SCA estimation employing the TKK SCA method is introduced in Publication [P6]. The publication presents the developed processing chain, explains the usage of the software and examines the limitations and operational aspects concerning it. The software is based on the research presented in publications [P1], [P2] and [P3] and can be used to produce SCA estimates supplemented with error estimates from Radarsat-1 ScanSAR Wide A satellite images for northern Finland.

REFERENCES

A. Arslan, W. Huining, J. Pulliainen, and M. Hallikainen, " Scattering from wet snow by applying strong fluctuation theory," Journal of Electromagnetic Waves and Applications, Vol.17, pp.1009-1024, 2003.

N. Baghdadi, Y. Gauthier, and M. Bernier, "Capability of multitemporal ERS-1 SAR data for wet snow mapping", Remote Sens. Environ., vol. 60(2), pp. 174–186, 1997.

N. Baghdadi, Y. Gauthier, M. Bernier, and J.-P. Fortin, ”Potential and limitations of RADARSAT SAR data for wet snow monitoring”, IEEE Trans. Geosci. Remote Sens., vol. 38(1) pp. 316-320, 2000.

M. Bernier, J. P. Fortin, and Y. Gauthier, “The potential of RADARSAT data to estimate the snow water equivalent based on results from ERS-1,” Proc. IGARSS’95, Firenze, Italy, pp. 1496–1498, 1995.

M. Bernier, and J.-P. Fortin, "The potential of times series of C-band SAR data to monitor dry and shallow snow cover", IEEE Trans. Geosci. Remote Sens., vol. 36, pp. 226-243, 1998.

P. Bevington and D. Robinson, ”Data reduction and error analysis for the physical sciences”, 2nd. ed., McGraw-Hill inc., 1992.

A. Chang, J. Foster, and D. Hall, “Nimbus 7 SMMR derived global snow-cover patterns,” Ann. Glaciol., vol. 9, pp. 39–44, 1987.

K. Chen, W. Wu, L. Tsang and J. Shi, "Emission of rough surfaces calculated by the integral equation method with comparison to three-dimensional moment method simulations," IEEE Trans. Geosci. Remote Sens. vol. 41, no. 1, pp. 90 - 101, 2003.

M. Eskelinen, J. Pulliainen, A. Kontu, H. Suokanerva, and S. Metsämäki, "The behaviour of snow and snow-free surface reflectance in the boreal forest area", Proc. 5th EARSeL Workshop, Bern, Switzerland, 11 - 13 February 2008.

A. Fung, ”Microwave Scattering and Emission Models and Their Applications”, Artech House, 1994.

T. Guneriussen, H. Johnsen, and K. Sand, ”DEM corrected ERS-1 SAR data for snow monitoring”, Int. J. Remote Sens. 17(1) 1996.

T. Guneriussen , K. Høgda, H. Johnsen, I. Lauknes, “InSAR for estimation of changes in snow water equivalent of dry snow,” IEEE Trans. Geosci. Remote Sens. vol. 39, no. 10, pp. 2101–2108, 2001.

D. Hall, G. Riggs, and V. Salomonson, "Development of methods for mapping global snow cover using moderate resolution imaging spectrometer data", Remote Sens. Environ., 54 (2), pp. 127–140, 1995.

D. Hall, J. Foster, D. Verbyla, A. Klein, and C. Benson, "Assessment of snow cover mapping accuracy in a variety of vegetation cover densities in central Alaska", Remote Sens. Environ., vol.66, pp. 129-137, 1998.

M. Hallikainen, F. Ulaby, M. Dobson, and M. El-Rayes, ”Microwave dielectric behavior of wet soil - Part I: Empirical models and experimental observations”, IEEE Trans. Geosci. Remote Sens. vol. 23: 25-34, 1985.

M. Hallikainen, F. Ulaby, and M. Abdelrazik, ”Dielectric Properties of Snow in the 3 to 37 GHz Range”, IEEE Trans. Antennas Propagat. vol. 34, no. 11, pp. 1329-1340, 1986.

M. Hallikainen and P. Jolma, “Comparison of algorithms for retrieval of snow water equivalent from Nimbus-7 SMMR data in Finland,” IEEE Trans. Geosci. Remote Sens., vol. 30, no. 1, pp. 124–131, Jan. 1992.

M. Hallikainen, P. Lahtinen, Y. Zhang, M. Takala, J. Pulliainen, "Feasibility of Satellite Ku-Band Scatterometer Data for Retrieval of Seasonal Snow Characteristics in Finland", Proc. IGARSS, Seoul, South-Korea, 25-29 July 2005.

M. Huttunen, “FEI Status report for EG Envisnow project, Work-package 7, Task 5”, June 2004.

IEEE Standard 521-2002, “IEEE Standard Letter Designations for Radar-Frequency Bands), 2002.

V. Jääskeläinen, "Remote Sensing of Snow by Microwave Radar", Licentiate of Science in Technology Thesis, Laboratory of Space Technology, Helsinki University of Technology, Espoo, 110 p. 1993.

J. Koskinen, L. Kurvonen, V. Jääskeläinen, and M. Hallikainen, ”Capability of radar and microwave radiometer to classify snow types in forested areas”, Proc. IGARSS’94, Pasadena, USA, pp.1283-1286, 1994.

J. Koskinen, J. Pulliainen, and M. Hallikainen, ”The use of ERS-1 SAR data in snow melt monitoring”, IEEE Trans. Geosci. Remote Sens. 35:601-610 1997.

J. Koskinen, S. Metsämäki, J. Grandell, S. Jänne, L. Matikainen and M. Hallikainen, "Snow monitoring using radar and optical satellite data," Remote Sens. Environ., vol. 69, no. 1, pp. 16-29, 1999.

J. Koskinen, “Snow Monitoring Using Microwave Radars,” Ph.D. Dissertation, Helsinki University of Technology, Laboratory of Space Technology, Report 44, Espoo, Finland, January 2001.

J.-P. Kärnä, N. Patrikainen, and J. Pulliainen, ”Automatic Rectification and Calibration Program for Radarsat Scansar Images”, Helsinki University of Technology, Laboratory of Space Technology, Report No. 61, Espoo, Finland, 2005.

R. Magagi, M. Bernier, and M.-C. Bouchard, “Use of ground observations to simulate the seasonal changes in the backscattering coefficient of the subarctic forest“, IEEE Trans. Geosci. Remote Sens., vol. 40: pp. 281-297, 2002.

R. Magagi, and M. Bernier, ”Optimal conditions for wet snow detection using RADARSAT SAR data”, Remote Sens. Environ. 84(2): 221-233, 2003.

E. Malnes and T. Guneriussen, “Mapping of snow covered area with Radarsat in Norway”, Proc. IGARSS, Toronto, Canada, 24-28 June, 2002.

S. Metsämäki, J. Vepsäläinen, J. Pulliainen, and Y. Sucksdorff, ”Improved linear interpolation method for the estimation of snow-covered area from optical data”, Remote Sens. Environ., vol. 82, pp. 64-78, 2002.

S. Metsämäki, S. Anttila, M. Huttunen, and J. Vepsäläinen, ”A feasible method for fractional snow cover mapping in boreal zone based on a reflectance model”, Remote Sens. Environ., vol. 95, pp. 77-95, 2005.

C. Mätzler, and E. Schanda, ”Snow mapping with active microwave sensors”, Int. J. Remote Sens., 15:409-422, 1984.

T. Nagler, and H. Rott, “Retrieval of wet snow by means of multitemporal SAR data“, IEEE Trans. Geosci. Remote Sens. 38: 754-765, 2000.

S. Nghiem and W. Tsai, "Global snow cover monitoring with spaceborne Ku-band scatterometer," IEEE Trans. Geosci. Remote Sens., vol. 39, no. 10, pp. 2118-2134, 2001.

Y. Oh, K. Sarabandi, and F. Ulaby, “An empirical model and an inversion technique for radar scattering from bare soil surfaces,” IEEE Trans. Geosci. Remote Sens., vol. 30, pp. 370-381, 1992.

J. Paavilainen, T. Siltala, and A. Vertanen, ”Digital land-use map, product spesification”, National Board of Survey, Department of Remote Sensing, 1992.

J. Piesbergen, F. Holecz, and H. Haefner, ”Snow cover monitoring using multitemporal ERS-1 SAR data”, Proc. IGARSS’95, Florence, Italy, pp.1750-1752, 1995.

J. Pulliainen, K. Heiska, J. Hyyppä, and M. Hallikainen, ”Backscattering properties of boreal forests at the C- and X-bands”, IEEE Trans. Geosci. Remote Sens. 32:1041-1050, 1994.

J. Pulliainen, P. Mikkelä, M. Hallikainen, and J.-P. Ikonen, “Seasonal dynamics of C-band backscatter of boreal forests with applications to biomass and soil moisture estimation,” IEEE Trans. Geosci. Remote Sens. 34:758–770, 1996.

J. Pulliainen, L. Kurvonen, and M. Hallikainen, “Multi-temporal behavior of L- and C-band SAR observations of boreal forest“, IEEE Trans. Geosci. Remote Sens. 37: 927-937, 1999.

J. Pulliainen, J. Koskinen, and M. Hallikainen, ”Compensation of forest canopy effects in the estimation of snow covered area from SAR data”, Proc. IGARSS, Sydney, Australia, 9-13 July 2001, pp. 813-815.

RADARSAT International (RSI), RADARSAT data products specifications. Report RSI-GS-026, version 3/0, 2000.

J. Raggam, A. Almer and D. Strobl, "A combination of SAR and optical line scanner imagery for stereoscopic extraction of 3-D data," Journal Photogram. Remote Sens., vol. 49, no. 4, 1994, pp. 11-21.

Y. Rauste, ”Methods for analysing SAR images”, VTT Research Reports 612, Technical Research Centre of Finland, Espoo, 1989.

H. Rott, “The analysis of backscattering properties from SAR data of mountain region,” IEEE J. Oceanic Eng. vol. 9:347-355, 1984.

H. Rott and T. Nagler, “Snow and glacier investigations by ERS-1 SAR—First results,” Proc. 1st ERS-1 Symp., 1993, ESA SP-359, pp. 577–582.

H. Rott and T. Nagler, “Capabilities of ERS-1 SAR for snow and glacier monitoring in alpine areas,” Proc. 2nd ERS-1 Symp., 1994, ESA SP-361, pp. 965–970.

V. Salomonson, and I. Appel, "Estimating fractional snow cover from MODIS using the normalized difference snow index" Remote Sens. Environ., 89(3), pp. 351-360, 2004.

J. Shi, and J. Dozier, ”Inferring snow wetness using C-band data from SIR-C’s polarimetric synthetic aperture radar”, IEEE Trans. Geosci. Remote Sens. 33: 905-914, 1995.

J. Shi, and J. Dozier, “Mapping seasonal snow with SIR-C X-SAR in mountainous areas,” Remote Sens. Environ., vol 59, pp. 294-307, 1997.

J. Shi, and J. Dozier, ”Estimation of snow water equivalence using SIR-C/X-SAR, part I: Inferring snow depth and particle size”, IEEE Trans. Geosci. Remote Sens. 38: 2475-2487, 2000.

J. Shi, “Snow water equivalence retrieval using X and Ku band dual-polarization radar,” Proc. IGARSS, Denver, Colorado, USA, July 31- August 4, 2006.

W. Stiles, and F. Ulaby, ”The active and passive microwave response to snow parameters: Part I – wetness”, J. Geophys. Research, (85):1037-1044, 1980.

R. Solberg, J. Amlien, H. Koren, L. Eikvil, E. Malnes and R. Storvold, “Multi-sensor/multi-temporal analysis of ENVISAT data for snow monitoring.” ESA ENVISAT & ERS Symposium 2004, Salzburg, Austria, 6-10 September 2004.

R. Solberg, R. Huseby, H. Koren and E. Malnes, “Time-series fusion of optical and SAR data for snow cover area mapping” Proceedings of EARSeL LIS-SIG Workshop, Berne, February 11-13, 2008.

R. Storvold, and E. Malnes, ”Snow covered area retrieval using Envisat ASAR wideswath in mountainous areas”, Proc. IGARSS, Anchorage, Alaska, 20-24 September 2004.

T. Strozzi, A. Wiesmann, and C. Mätzler, “Active microwave signatures of snow covers at 5.3 and 35 GHz”, Radio Science 32:479-495, 1997.

M. Tedesco and J. Miller, "Northern Hemisphere Snow-Covered Area Mapping: Optical Versus Active and Passive Microwave Data", IEEE Geosci. Remote Sens. Lett., vol. 4, no. 2, pp. 221-225, April 2007.

L. Tsang, J. Kong, and R. Shin, “Theory of Microwave Remote Sensing”, New York: Wiley, 1985.

F. Ulaby, R. Moore, and A. Fung, ”Microwave Remote Sensing, Active and Passive”, Volume II. Reading, Addison Wesley, 609 p. 1982.

F. Ulaby, R. Moore, and A. Fung, ”Microwave Remote Sensing, Active and Passive”, Volume III, Artech House, 1100 p. 1986.

B. Vehviläinen, ”The watershed simulation and forecasting system in the National Board of Waters and Environment”, Publications of the Water and Environment Research Institute, No.17, National Board of Waters and the Environment, Finland, 1994.

D. Vikhamar, and R. Solberg, "Subpixel mapping of snow cover in forests by optical remote sensing", Remote Sens. Environ., 84(1), pp. 69-82, 2003.

U. Wegmüller, C. Werner, and T. Strozzi, ”SAR Interferometric and Differential Interferometric Processing Chain”, Proc. IGARSS'98, Seattle, USA, vol.2, pp.1106-1108, 1998.

Ilmatieteen laitos
Erik Palménin aukio 1, Helsinki
tel. (09) 19 291
www.fmi.fi

ISBN 978-951-697-689-4 (paperback)
ISBN 978-951-697-690-0 (pdf)
ISSN 0782-6117

Yliopistopaino
Helsinki, 2009